**University of Liège**
Department of Aerospace & Mechanical Engineering
Computational & Multiscale Mechanics of Materials

Université de Liège

# Development and numerical validation of a 2-scale computational tool to describe the mechanical behavior of nanocrystalline metals

by

Vincent Péron-Lührs

Submitted in fulfillment of the requirements for the degree of
Doctor in Engineering Sciences

January 2014

| | |
|---|---|
| Ludovic NOELS | Thesis Supervisor |
| Frédéric SANSOZ | Committee Member |
| Antoine JÉRUSALEM | Committee Member |
| Laurent STAINIER | Committee Member |
| Jacqueline LECOMTE-BECKERS | Committee Member |
| Philippe GHOSEZ | Committee Member |
| Anne-Marie HABRAKEN | Committee Member |

# Contents

# Abstract

This thesis presents a two-scale numerical tool aimed at predicting the mechanical behavior of nanocrystalline metals. To this end, a finite element model called direct numerical simulation, is calibrated (or atomistically-informed) using the quasicontinuum method (QC). The constitutive model is based on the mechanical behavior of two constitutive elements: the grains (or bulk crystals) and the grain-boundaries (GBs). The grains, governed by a forest dislocation-based hardening model, are calibrated according to their size and orientation by means of nanoindentation tests. GBs, taking the form of surfaces of discontinuities embedded in the continuum, are calibrated with QC according to their misorientations by applying tensile and shear loadings to bicrystals, allowing for the extraction of the elasto-plastic laws related to the GB opening and to the GB sliding behaviors, respectively. The method is numerically validated against full atomistic simulations. It is found that this two-scale method is able to predict the behaviors of the nanocrystals according to their specific GB character distributions and mean grain sizes, and to capture the competition between intragranular and intergranular plasticity. This thesis demonstrates the ability of such a method to also predict the weakest points and the direction of crack propagation in nanocrystalline structures. A simplified calibration strategy aimed at reducing the computational cost for structures consisting of a substantial number of grains is also proposed. Moreover, this work presents a possible way to improve the model with respect to the GB maximum shear stresses by introducing nano-scaled voids within GBs, opening the way to a better understanding of mechanisms taking place in defective GBs.

# Acknowledgments

Je tiens à remercier le Prof. Ludovic Noels pour ses conseils avisés et son incroyable disponibilité tout au long de ce travail de thèse.

Je remercie le Prof. Laurent Stainier de m'avoir offert la possibilité de me lancer dans cette thèse.

Je remercie tout spécialement le Prof. Frédéric Sansoz pour son accueil chaleureux à son laboratoire du Vermont et pour son aide particulièrement précieuse dans ce travail.

Je remercie le Prof. Antoine Jérusalem pour son accueil à Madrid et pour ses excellents conseils aussi bien personnels que professionnels.

Je remercie plus généralement les membres du personnel du LTAS pour leur aide et leur gentillesse.

Je remercie ma grande soeur pour ses conseils éclairés et je lui en veux un peu quand même d'avoir mis la barre aussi haut :)

Je remercie mes amis Neil, Yannick, et Victor qui m'ont accompagné pendant toutes ces années et ont su me supporter et trouver les mots dans les moments difficiles.

Et puis, je ne peux pas m'empêcher de remercier tous mes amis avec qui je me suis amusé pendant tout ce temps et qui m'ont permis de voir les choses sous un angle festif et sympathique. Je pense notamment à Agnieszka, Virginie, Marie, Sarah, Guillaume, Gilouto, Vincent, Tom, JC, Benito, Charly, Guara, James, Olga, Henri, Chris, et Christina.

# Nomenclature

# List of symbols

| | |
|---|---|
| $a^{\alpha\beta}$ | Interaction matrix coefficients |
| $\boldsymbol{a}_\alpha$ | Covariant basis vector in the grain-boundary element referential |
| $b$ | Burgers vector |
| $B_0$ | Region occupied by the body in the initial configuration |
| $B_0^g$ | Region occupied by grain $g$ in the initial configuration |
| $B$ | Region occupied by the body in the current configuration |
| $\underline{\boldsymbol{b}}$ | Body forces |
| $C_{11}, C_{12}, C_{44}$ | Elastic constants |
| $d$ | Grain diameter |
| $D$ | Damage parameter of a grain-boundary |
| $F_i$ | Energy embedding atom $i$ |
| $G$ | Shear modulus of a grain-boundary |
| $g_0$ | Initial critical resolved shear stress |
| $g^\alpha$ | Critical resolved shear stress on slip system $\alpha$ |
| $\dot{g}^\alpha$ | Flow stress on slip system $\alpha$ |
| $h$ | Grain-boundary width |
| $h^{\alpha\alpha}$ | Hardening diagonal modulus of slip system $\alpha$ |
| $h_{GB}$ | Pseudo grain size/distance grain-boundary to indented surface |
| $\boldsymbol{I}$ | Unity tensor |
| $l$ | Distance between two forests of dislocations |
| $m$ | Strain-rate sensitivity exponent in grain |
| $\underline{\boldsymbol{n}}$ | Grain-boundary surface normal in the deformed configuration |
| $n_\alpha$ | Density of obstacles in system $\alpha$ |

*continued on next page*

continued from previous page

| | |
|---|---|
| $\underline{\boldsymbol{N}}$ | Grain-boundary surface normal in the initial configuration |
| $S$ | Midsurface in the grain-boundary element |
| $S^+$ | Facet corresponding to the tetrahedra on the positive side of a grain-boundary |
| $S^-$ | Facet corresponding to the tetrahedra on the negative side of a grain-boundary |
| $s^\alpha$ | Strength of the obstacle in slip plane $\alpha$ given by a pair of forest dislocations |
| $p$ | Centrosymmetry parameter |
| $V$ | Void volume fraction in grain-boundary |
| $\underline{\bar{\boldsymbol{t}}}$ | Grain-boundary traction |
| $\partial B_0$ | External boundary of a polycrystal aggregate in the initial configuration |
| $\partial B_0^{ext}$ | External exposed boundary of a polycrystal aggregate in the initial configuration |
| $\partial B_0^g$ | Boundary of grain $g$ in the initial configuration |
| $\partial B_0^{gb}$ | Grain-boundary surface in the initial configuration |
| $\underline{\boldsymbol{\delta}}$ | Displacement jump at the grain-boundary |
| $\delta_c$ | Strain-to-failure opening of the grain-boundary |
| $\underline{\boldsymbol{\delta_n}}$ | Normal component of the displacement jump at the grain-boundary |
| $\underline{\boldsymbol{\delta_s}}$ | Sliding component of the displacement jump at the grain-boundary |
| $\Delta\Psi$ | Grain-boundary misorientation |
| $\underline{\underline{\boldsymbol{\epsilon}}}$ | Strain at the grain-boundary |
| $\epsilon_0$ | Grain-boundary reference plastic strain |
| $\underline{\underline{\boldsymbol{\epsilon_n}}}$ | Normal component of the grain-boundary strain |
| $\overline{\epsilon_p}$ | Grain-boundary effective plastic strain |
| $\underline{\underline{\boldsymbol{\epsilon_s}}}$ | Sliding component of the grain-boundary strain |
| $\dot{\gamma_0}$ | Reference shear strain rate |
| $\gamma_{sat}$ | Saturation shear slip |
| $\dot{\gamma^\alpha}$ | Current shear strain rate on slip system $\alpha$ |
| $\gamma^\alpha$ | Shear strain on slip system $\alpha$ |

*continued on next page*

| continued from previous page | |
|---|---|
| $\gamma_c^\alpha$ | Characteristic shear strain on slip system $\alpha$ |
| $\mu$ | Shear modulus in grains |
| $R_{ij}$ | Distance between atoms $i$ and $j$ (EAM theory) |
| $\rho_{h,i}$ | Host electron density at atom $i$ (EAM theory) |
| $\rho$ | Background electron density (EAM theory) |
| $\rho_{sat}$ | Saturation dislocation density (Ref. A) |
| $\rho_0$ | Material density in the initial configuration (Ref. A) |
| $\rho$ | Material density in the current configuration (Ref. A) |
| $\rho^\alpha$ | Dislocation density in slip system $\alpha$ (Ref. A) |
| $\underline{\underline{\boldsymbol{\sigma}}}$ | Cauchy stress tensor |
| $\sigma_0$ | Grain-boundary initial yield stress in sliding |
| $\sigma_c$ | Critical stress in grain-boundary opening |
| $\overline{\underline{\underline{\boldsymbol{\sigma}}}}^{op}$ | Grain-boundary opening stress component |
| $\overline{\underline{\underline{\boldsymbol{\sigma}}}}^{sl}$ | Grain-boundary sliding stress component |
| $\sigma_{max_0}$ | Maximum shear strength of a perfect grain-boundary |
| $\sigma_{max}$ | Maximum shear strength of a defective grain-boundary |
| $\sigma_p$ | Yield stress corresponding to $\bar{\epsilon}_p$ |
| $\sigma_v$ | Void-induced stress |
| $\phi_{ij}$ | Core-core pair repulsion between atoms $i$ and $j$ (EAM theory) |
| $\underline{\boldsymbol{\varphi}}$ | Deformation mapping |
| $\underline{\boldsymbol{\varphi}}^+$ | Deformation mapping for the top surface of the grain-boundary |
| $\underline{\boldsymbol{\varphi}}^-$ | Deformation mapping for the bottom surface of the grain-boundary |
| $\underline{\tilde{\boldsymbol{\varphi}}}$ | Mean deformation mapping of the grain-boundary |
| $\tau^\alpha$ | Resolved shear stress on slip system $\alpha$ |
| $\tau_c^\alpha$ | Characteristic resolved shear stress on slip system $\alpha$ |

# Abbreviations

# Abbreviations

| | |
|---|---|
| 2D | Two-dimensional |
| 3D | Three-dimensional |
| BCC | Body-centered cubic |
| BEM | Boundary element method |
| CPU | Central processing unit |
| CPFE | Crystal plasticity finite-element method |
| DC | Direct electric current |
| DNS | Direct numerical simulation |
| CSL/$\Sigma$ | Coincidence site lattice GB |
| CRSS | Critical resolved shear stress |
| EAM | Embedded-atom method |
| ECAP | Equal channel angular pressing |
| ED | Emission of dislocations from periodic defects |
| EV | Emission of dislocations from voids |
| FCC/fcc | Face-centered cubic |
| FEM | Finite-element method |
| GB | Grain-boundary |
| GBCD | Grain-boundary character distribution |
| GBE | GB engineering |
| HA | High-angle |

*continued on next page*

| continued from previous page | |
|---|---|
| HAB | High-angle boundary |
| HC | Hexagonal compact |
| HP (effect) | Hall-Petch (effect) |
| HP | Homogeneous and partial GB migration |
| HS | Homogeneous shuffling |
| HT | Homogeneous and total GB migration |
| IP | Inhomogeneous and partial GB migration |
| LA | Low-angle |
| LAB | Low-angle boundary |
| MC | Microcrystalline material |
| MD | Molecular dynamics |
| MS | Molecular statics |
| NC/nc | Nanocrystal |
| PS | Partial shuffling |
| QC | Quasicontinuum |
| RHP (effect) | Reverse Hall-Petch (effect) |
| RVE | Representative volume element |
| SPD | Severe plastic deformation |
| SMAT | Surface mechanical attrition treatment |
| TB | Twin boundary |
| TJ | Triple junction |
| UFC | Ultrafine crystalline material |

# Chapter 1

# Introduction

## 1.1 State of the art

The discovery of metals and their alloys has greatly contributed to the evolution of humankind, allowing us to move from cave-dwelling humans to today's modern society. The mastery of this material took time. We first broke rocks to extract the shiny material, we forged and gave it shapes adapted to our needs, as hunting weapons or agricultural tools. We mixed copper with tin to make it harder compared to pure copper (Bronze Age). Iron then came into play (Iron Age), providing lighter, harder and less expensive tools. Since then, this will to improve metal's features has not abated.

About fifty years ago, Hall and Petch discovered how to strengthen metals by reducing the size of their crystallites (or grains). This discovery took the name of Hall-Petch (HP) effect [34, 67]. In 1968, Hirth and Lothe [35], who were focusing their research efforts on dislocation study, proposed to explain this HP effect by using a pile-up model assuming that dislocations were stopped at the grain boundaries (GBs), hence strengthening the material. A few years later, highly cold wire drawing resulted in alloys presenting an extraordinary strength compared to usual coarser grained materials [68]. This peculiar behavior was due to the nanosized grains that make up these alloys. This discovery probably inspired Gleiter [29] who declared that making nanocrystalline materials might open up the path toward significant improvements of the mechanical properties of metals and alloys. Gleiter's work predicted these properties: fracture resistance and ultrahigh yield strength, better wear resistance, and possible superplastic mechanical behavior. Three new material classes were named according to the grain sizes. We now talk about nanocrystalline (NC) materials when the sample presents at least one dimension smaller than 100 nm [30]. The term ultrafine crystalline (UFC) materials is used from 100 nm to 1 $\mu$m. Finally, when the average grain size is larger than 1 $\mu$m we use the term microcrystalline (MC) materials. At first these structures were studied experimentally, however the material processing appears to be a limiting factor in a full understanding of the material's behavior, motivating the use of numerical models.

### 1.1.1 Experimental approach

When processing such materials in order to capture the intrinsic material response, it is essential to control different features. It is necessary to control the defect concentration, the grain size distribution, the crystallographic orientations, the porosity, the residual stresses and the internal strains. Among all the developed techniques, three of them hold the most prominent ability to control these intrinsic properties: electrodeposition, severe plastic deformation (SPD), and cluster deposition techniques.

The electrodeposition technique is the oldest one which makes it possible to obtain the following intrinsic properties. Electrodeposition has the advantage of producing a large number of grain nuclei, which enables the achievement of a significant reduction of the grain size [58]. Growth texture with a grain size of 30 nm can be obtained using direct electric current (DC) electrolysis in the case of Ni [19]. Texture-free and pore-free NC metals with grain sizes below 20 nm have also been obtained using pulse procedures [58, 54].

The SPD technique, in turn, has the ability to provide perfectly dense bulk materials which is very interesting for the mechanical properties [95]. Conventional SPD techniques often produce UFC with grain sizes larger than 100 nm rather than NC and some additive processes, such as the surface mechanical attrition treatment (SMAT) are needed to refine the grains in the nanometer range [53]. Nevertheless, these SPD techniques are also known for the wide grain size distribution they produce, which acts as a limiting factor on the understanding of NC intrinsic properties.

Finally, the cluster deposition techniques or nanocluster techniques provide grain sizes of just a few nanometers with a narrow grain distribution [14]. It also allows, by judiciously choosing the substrate, the texture of the sample to be "tailored", which constitutes a particularly powerful tool for texture analysis.

#### Grain-boundary engineering

It is partially due to these aformentioned processing techniques that huge progresses in engineering microstructures at the nanoscale have been made recently. Nanostructuring also offers the possibility to improve mechanical properties such as strength and hardness [8] and ductility [55], among other interesting mechanical properties, and allows for a better understanding of how to control the strain-rate and temperature strength dependencies [85, 13, 99]. Furthermore it is worth noting that other properties such as a higher electrical conductivity can be achieved using nanoscale growth twins [54]. Watanabe was the first person to propose the concept of "GB design" [101], a concept that took the name of "GB engineering" (GBE) and is now well established [102]. Because GBs were identified as preferential sites for crack nucleation and propagation, reinforcing them appeared as a way to strengthen the material. The idea was to improve the resistance to intergranular fracture by increasing the proportion of strong GBs. The success of these techniques [52] was attributed to the high proportion of "special GBs". It is now known that these special boundaries belong to two classes: low-angle boundaries

(LABs) and coincident site lattice GBs (CSLs). On the one hand, LABs are the GBs that present low misorientations angles, lower than than 10 degrees [75, 4], or between 9 and 14 degrees [86]. Note that when a GB presents a higher misorientation angle, it is called a random boundary or a high-angle boundary (HAB), and its properties are not considered as specials. On the other hand, the CSL type nomenclature is represented by a sigma ($\Sigma$) followed by the reciprocal density of coincident atoms in the GB interface. CSLs[1] are considered as specials in terms of properties only if a periodic structure in the boundary plane is maintained [87]. Nowadays, only $\Sigma 3$ and $\Sigma 3^n$ types are the special GBs processed experimentally to improve the mechanical properties of NC materials [70].

While the increased fraction of special boundaries contributes in substantial enhancements, like for instance corrosion resistance [62, 52], creep resistance [43], and stress corrosion cracking resistance [62, 9], the grain boundary network topology cannot be properly described without considering triple junction (TJ) network or distribution, which is particularly important in hindering crack propagation mechanisms [69]. TJs can be classified according to the number of special boundaries that coordinate them. Type 0-CSL TJ consists of 3 HABs, and type 1-CSL, 2-CSL and 3-CSL have 1, 2 and 3 special boundaries respectively. The fraction of special boundaries controls the TJ mechanical behavior. From the experimental point of view, the thermomechanical processing allows for the reorganization of GBs toward lower energy configurations, i.e. low CSLs, and opens the way to a relative control of the triple junction distribution [47]. However, the experimental control of this distribution is still in its infancy.

### Limits of the experimental approach

The evolution of the experimental techniques has allowed the highlighting of the impact of nanostructuring polycrystals on the macroscopic behavior of these materials, and has resulted, inter alia, to the advent of the GBE concept. This latter technique aims to improve the mechanical properties of polycrystals by creating the appropriate GB network and is becoming increasingly popular. However, the experimental approach requires fastidious material manufacturing and preparation. These processes are also particularly expensive and time consuming. Moreover, these techniques are still unable to access the structural parameters, or so-called "hidden parameters", that can give accurate insights on the mechanical properties of NC materials. During the past years the wide range of new experimental researches flourishing in this area were not truly representative of the tremendous potential of these materials because of the difficulty met for properly preparing NC samples [47]. This has motivated the development of numerical approaches.

[1]The terms low-$\Sigma$ CSLs and high-$\Sigma$ CSLs were first used to determine whether a given GB would present special properties or not. However, a lower $\Sigma$ value, i.e. involving a higher density of coincident atoms in the GB interface, is eventually not a sufficient criterion as special properties were observed for high-$\Sigma$ values and sometimes not observed for low-$\Sigma$ values [69].

### 1.1.2 Numerical approach

In parallel with these experimental techniques, the numerical tools appeared to be very efficient methods to predict the possible deformation mechanisms taking place in such nanostructures. Consequently an increasing interest in numerical approaches has arisen. In fact, because of the small scales involved, only this last approach can inform directly on GBs, TJs, or internal stress distribution, among other fundamental structural parameters of the nanoscale.

#### Molecular dynamics

Molecular dynamics is a computer simulation method created in the late 50s [1]. This method allows for the prediction of the movement of atoms on the basis of force fields derivated from potential energies defined by solving the Schrödinger equation.

MD has been a powerful tool in unveiling the peculiar behaviors taking place at the nanoscale, most of the time unreachable experimentally. It is now very well known that NCs are grain size dependent and MD helped in highligting the reasons for this dependency. In the normal polycrystalline regime, plasticity is known to be governed by dislocation-dislocation interactions, i.e. by intragranular plasticity. Then, when decreasing the grain size, a fundamentally different dislocation activity is triggered. Indeed, between 12 to 30 nm, all simulations indicate first a dislocation-based intragranular deformation mechanism, and second, that dislocations are also emitted from the GBs [82, 108, 97, 105, 76, 17, 81]. The propagation of dislocations emitted from these two sources of dislocations leads to pile-ups at GBs which result in a consequent hardening of the material, responsible for the HP effect. Below 10 to 12 nm, the intragranular dislocation propagation becomes increasingly more difficult and plasticity is found to be dominated by intergrain deformation mechanisms [96, 47], leading to a reduction of the yield and flow stresses. This phenomenon, implying the existence of a strongest grain size [110] for a given material, is known as the reverse or inverse HP effect (RHP) [39] and was also observed experimentally [22].

MD nonetheless suffers from the requirement to consider the dynamics of all atoms one by one, which imposes drastic limitations on the size of the sample simulated. The MD method is also limited to simulations with very high-strain rates, and is therefore suitable for fast loading such as shocks for instance. Other numerical methods, such as the finite element method, have been developped and make it possible to transcend the length-scale and time-scale limits of MD.

#### Finite element methods

Several techniques using continuum models and in particular the finite element method (FEM) have been developed and used to describe the mechanical behaviors of polycrystals. The FEM approach is a traditional approximation of the weak form used to describe the mechanics of materials [37, 111]. In this framework, materials are

considered to be infinitely divisible media. Becoming more conscient about the importance of understanding the underlying mechanisms taking place at the lower length scales in the matter, Pierce has developed in 1982 [63] a multiscale method in order to treat the crystal plasticity. His method, called the crystal plasticity finite element method (CPFE) has been used as a multimechanism and multiphysics platform. Since then, this approach has been applied to various crystal mechanical problems, see the overview of Roters et al. [72]. In this framework, the FEM is used as a variational solver for the underlying constitutive equations treating the anisotropic elasto-plastic deformation of different types of lattice defects, i.e. dislocations, disclinations, twins and more generally GBs. These constitutive equations governing the deformation may be incorporated in two different kinds of models. Either the model is said to be "local" and the stresses are computed on the basis of the displacement field only, or the model is said to be "non-local" and is also based on the strain-gradient. In other words, the description of the deformation of the material in the local models is achieved by using higher order terms. Thus according to the approach, local or non-local, considerations of crystal defects and the associated mechanisms are treated in a different manner.

In the local approach case, when dealing with NCs, the integration of the GBs has been treated in a variety of ways. Grain interior and boundary processes were included in a homogenized way [41, 26]. GBs were also explicitly treated as continuum regions with different properties [85, 104] or interfaces elements were introduced in the finite element mesh [103, 100]. These studies have been mainly limited to two-dimensional (2D) analyzes focused on the ability of the continuum approach to describe the grain size dependency [104, 100], the strain localization [27, 100] and the failure process [104, 103]. Also, three-dimensional (3D) models have been proposed for analysing polycrystalline materials [10, 36] with the desire to be more realistic and to complement experimental investigations. This was also motivated by the complex three-dimensional mechanisms taking place in these materials, such as the geometry influence on the microcraking evolution, competition between different failure modes. Jérusalem and Radovitzky [39] proposed a finite element formulation of the continuum three-dimensional problem. This model explicitly describes the deformation of polycrystal grains and the GBs are considered as surfaces of discontinuities with a finite thickness embedded in the continuum. GB sliding was incorporated in the model to demonstrate its hability to reveal the softening of NC metals with decreasing grain sizes (RHP effect). However, a unique arbitrary constitutive law was used to characterize all the GBs, despite the different natures of the GBs (HAB, LAB, or $\Sigma$). An alternative is to use judicious distributions of properties in GBs based on statistics to describe the mechanical behavior of GBs in polycrystalline materials [44]. This approximation of the nature of GBs of NC metals, which makes the specific behaviors of the textures difficult to be captured, is due to the lack of data available in the literature. As a consequence, the description of the mechanical behavior of GB networks has mainly been studied through arbitrary or statistical techniques. A finer and more accurate description appears as a necessary step for an increased understanding of the deformation mechanisms involved in nanocrystalline

materials. Recently, Benedetti [3] developed a three-dimensional formulation for the analysis of intergranular degradation and failure in polycrystalline materials based on the boundary element method (BEM). The BEM is an alternative to the FEM that has proven its efficiency for physical and engineering problems [106, 2]. Nervertheless, this latter approach still focuses on MCs and not on NCs.

While some of the mechanisms taking place at GBs can be reproduced in the local framework, deformation mechanisms referred to as core contributions, i.e. for instance, the emission or absorption of dislocations by GBs, requiring to deal with higher order terms, cannot be taken into account with the local approaches. Thus this constitutive framework appears insufficient to describe the huge complexity of the crystal plasticity. In fact, these theories must be of higher orders, not only by incorporating the strain gradients but also by having higher order stresses that are work conjugate to the strain gradients, making possible the modelling of extra boundary conditions. Gurtin and Anand [32] have first developped a small-deformation strain-gradient theory plasticity for isotropic materials in the absence of plastic rotation, resulting in a tensorial second-order partial differential equation for the plastic strain, and then have extended the model to large-deformation [31]. Gurtin has recently developed a theory of rate-independent single-crystal plasticity at small length scales [33]. In this latter framework, microscopic stresses are related to the tangential gradients on the individual slip systems and the initial-boundary values are placed in a variational setting. As a result, this model can determine the active slip systems and the location of the elasto-plastic interface at any time. However, in the approach of Gurtin, higher order stress quantities can change discontinuously for bodies subjected to arbitrarily small load changes, causing physical deficiency. Based on the work of Gurtin, the elasto-plastic theory of crystal defect field presented in Ref. [23, 24, 93] accounts for the translational and rotational incompatibility of the lattice associated with dislocations and disclinations in a continuous fashion. As a result, these models are able to take into account the dislocation-GB interactions, thus capable of capturing size-dependent behaviour of metals at the micron scale. Also, in the theories proposed by Muhlhaus and Aifantis [57], and Fleck and Hutchinson [20], the strain-gradients induced by the deformation phenomena at the microscale are taken into account by generalizing the classical J2 flow theory of plasticity. Nevertheless, thermodynamic requirements on plastic dissipation are not always satisfied. Other work [38] intends to rectify this physical deficiency. As a summary, although these models are of clear interest to describe the crystal defects mechanics, higher orders mechanics still needs to be improved. Based on the J2 flow theory of plasticity, these frameworks remain isotropic, adapted only to the microscale, i.e. not the nanoscale, and cause problems from a physical point of view. They finally remain oversimplified on several accounts due to the difficulties encountered when determining physical parameters such as, for instance, the elastic constants for the couple-stresses that are yet unknown. The quasicontinuum method, presented in the next Section, appears as a suitable technique to determine some of these parameters.

### The quasicontinuum method

The quasicontinuum(QC) method was developed by Tadmor, Ortiz, and Phillips, see Ref. [91], and is a molecular statics technique finding the solution of equilibrium atomic configuration by energy minimization, given externally imposed forces or displacements. As for MD, the potential energies are defined by solving the Schrödinger equation. Also, comparatively to the MD that is a fully-atomistic technique and presents length-scale limits, the QC method does not suffer from this problem. Indeed, aimed at modeling atomistic systems, the problem is modeled without explicitly representing every atoms in the cell; here, regions of small deformation gradients are treated as continuum media by a finite element method. In this scheme, the connection between continuum and full atomistic is made in a seamless manner, i.e. that there is no discontinuity in the energy state at the continuum/atomistic frontier. Indeed, the QC uses continuum assumptions to reduce the degrees of freedom and computational demand without losing atomistic details in regions where it is required. In this manner the cell size can be large enough to provide realistic boundary conditions. This method has been particularly useful, for instance, in predicting the GB mechanical behavior under shear and tension [79, 80]. A detailed overview of the QC implementation is available in Ref. [56]. We present in this Section the embedded atom method (EAM) used to determine the potential energies governing the interactions between atoms in the QC method. We then expose the limitations of the QC method in order to understand its relevance in the framework of this thesis work.

#### The embedded atom method

The EAM potential provided by Foiles et al. [21] for copper was used for all QC simulations presented in this thesis. In this latter work, the authors have showed that within the framework of the density-functional theory, the total energy for an arbitrary arrangement of nuclei can be written as a unique functionnal of the total electron density. Here, the total energy can be approximated by

$$E_{tot} = \sum_i F_i(\rho_{h,i}) + \frac{1}{2}\sum_i \sum_{j(\neq i)} \phi_{ij}(R_{ij}) \tag{1.1}$$

In this expression, $\rho_{h,i}$ is the host electron density at atom $i$ due to the remaining atoms of the system, $F_i(\rho)$ is the energy to embed atom $i$ into the background electron density $\rho$, and $\phi_{ij}(R_{ij})$ is the core-core pair repulsion between atoms $i$ and $j$ separated by the distance $R_{ij}$. The electron density being

$$\rho_{h,i} = \sum_{j(\neq i)} \rho_j^a(R_{ij}) \tag{1.2}$$

where $\rho_j^a(R)$ is the electron density contributed by atom $j$. Using equation (1.1) leads to a cutoff distance of 4.950 Å for copper.

**The QC limitations**

The QC method available on www.qcmethod.com and which is used in the context of this thesis is a freeware submitted to certain limitations that are enumerated in the following.

- This code is limited to 2D problems that can be described with the following displacement field

$$u_x(x,y), u_y(x,y), u_z(x,y)$$

- Despite this 2D constraint, every calculation is performed in 3D. This amounts to simulating a slice whose thickness is equal to the minimum crystallographic distance in the out-of-plane direction (Plane State of Stress).

- The code is limited to crystalline materials with a simple lattice structure as the face-centered cubic (FCC) and body-centered cubic (BCC) structures. It is therefore not possible with this version of QC to simulate complex structures such as hexagonal compact (HC) ones or asymmetric units containing several species. Note that it is possible to simulate systems with multiple structures and species if they are in separate grains.

- This code is a quasi-static model based on energy minimization. It can be used to study the equilibrium structures at zero temperature, but does not allow the simulation of dynamic processes and effects at given finite temperatures due to the current version of the implementation of the software.

- The atomic interactions are limited to empirical potentials. The total energy of the system is equal to the sum of the energies of the atoms in the system.

- These limitations concern the QC version considered here. In fact, the extension to 3D [71], to complex crystals [92, 15], or to problems at finite temperatures [18] are subject of various studies.

Finally, the QC method is not adapted for large NC simulations and would degenerate to a full atomistic method as the small size of the grains requires all the atoms to be modelled. The QC method would thus suffer from length-scale limitation in the NC context.

## 1.2 Contributions

In this thesis, we develop a numerical tool which provides the advantages of both methods (Atomistic model and FEM), that is, keeping the powerful prediction ability

of atomistic models without suffering from dractic limitations on the size of the samples studied. To predict the NCs mechanical behaviors according to their specific texture, also called grain-boundary character distribution (GBCD), an FEM algorithm with embedded surfaces as GBs, called direct numerical simulation (DNS), is calibrated by using the QC method. In this way, we provide a FEM algorithm atomistically-informed, i.e. a two-scale model. The ability of the DNS model to predict the mechanical behavior of NCs is based on the constitutive behavior of two elements, the grains on the one hand, and the GBs on the other. As outlined above, the nanomecanisms involved in these two elements are of different natures and must therefore be calibrated by a different manner.

With regard to grains, plasticity is governed by dislocation motions, by dislocation-dislocation and GB-dislocation interactions. In addition, the grain size effect induced by this latter interaction (GB-dislocation) must also be considered as being able to faithfully reproduce the mechanical behavior of grains. The explicit formulation described in Ref. [45], enabling large scale computations, is adopted for the intragranular FCC polycrystal plasticity constitutive model. In this model, the constitutive response of grains is described with a forest dislocation-based hardening model. Note that we use the parameters available in the literature [11] to evaluate the dislocation-dislocation interactions. By constrast, our contribution lies here in the development of a calibration model enabling the prediction of the initial critical resolved shear stress (CRSS) required to activate the FCC slip systems responsible for dislocation motions in grains, while taking into account both the size effect and the grains crystallographic orientations. To this end, the CRSS of FCC slip systems are determined by means of nanoindentation tests with QC. Also, the size effect is captured by adding a GB in the vicinity of the indenter and by vaying the distance GB-indented surface, which distinguishes the current study from the one presented in Ref. [90] by QC designers. It is also worth noting that for this GB-dislocation interaction, both LAB or HAB types are used to reflect the size effect in both LA- or HA-type GBCDs or textures. On the basis of this calibration process, a higher CRSS is found, and thus a grain hardening is predicted when decreasing the grain size below 4 nm, highlighting the increased difficulty for dislocations to move in such small grains.

In the FEM developped up here, GBs are treated as surfaces of discontinuities embedded in the continuum, following the work presented in Ref. [39]. In this latter work, one arbitrary constitutive law was used to describe all the GBs and was limited to GB sliding only. On this basis, the model is implemented with decohesion/opening ability for GBs in order to allow for the direction of the intergranular crack propagation to be captured. By applying shearing and tensile loadings on bicrystals using the QC method exposed in Ref. [79, 80], the elasto-plastic parameters governing the GB responses are determined according to their specific misorientations. It should also be noted that the determination process to obtain these GB parameters is automated in the framework of this thesis, i.e. automation of the research of the best GB energy configuration and setting of the GBs simulation parameters. Moreover, this GB sliding and opening calibration process provides an opportunity to define the evolution of these parameters

according to their misorientations, something that is unprecedented. In particular, the identified trends concern yield stresses, Young and shear moduli, GB energies, critical stresses, strain-to-failures and GB widths. Critical stresses and strain-to-failures are found to be significantly higher in LABs than in HABs. In addition, HABs are found to be wider than LABs. Although adaptable to other tilt axes, this work only considers GBs with the $[1\bar{1}0]$ tilt axis. This is due to the 2D nature of the QC software and makes this framework solely suitable for addressing columnar thin films. Although the limit arises from the QC model, the FEM used in this work is however able to deal with finite-temperature 3D problems for a large range of strain-rates, and this in the case of more general crystalline solids.

Once the two-scale model is completely calibrated (grains and GBs), it is tested on a 16-grain and 34-GB representative volume element (RVE) for different mean grain sizes and different textures (LA and HA). Then the model is numerically validated by comparing it in the same loading conditions to a fully-atomistic QC model. We demonstrate that the global stiffness of the NC is highly dependent on the width and the nature of the GBs that constitute it. We show that setting HABs widths to a unique value of 1.5 nm does not induce any discrepancy in the NC response. Conversely, LABs appear to be more sensitive to their widths calibration. In particular, we show that the direction of the crack propagation is highly dependent on the width calibration in the LAB case. It is found that both models predict the same trends concerning not only the homogenized Young moduli and yield stresses, but also the weak points of the GB networks considered and the direction of the cracks propagation. Moreover, the model demonstrates its ability to predict the behavior of these textures according to their specific natures. In addition, the model is able to capture the reverse Hall-Petch effect [82], i.e. the softening of the NC metals when decreasing the grain size or, in other words, it is able to predict the switching from an intragranular plasticity toward an intergranular plasticity.

We then illustrate the ability of the model to address structures presenting a large number of grains and GBs. To this end, we apply the method to a HA-type dogbone consisting of 103 grains and 251 GBs. For that study, the GBs are not calibrated from QC simulations but from a fitting of the trends resulting from previous GB simulations with QC. Through this HA-type dogbone simulations, the method highlights notably the importance of the competition between intragranular and intergranular plasticity when dealing with such small grains.

Despite the care devoted to the calibration of the two-scale model, the predictions of NCs behaviors remain nevertheless overvalued compared to experiments and MD simulations. This is mainly due to the 2D nature of QC and also because no thermally activated processes are accounted for in the QC simulations. Also, the GBs simulations only address the issue of GBs presenting a perfect crystallographic organisation. In fact, no defects, kinks, or nanovoids are included in the GB response. Thus an effort was made to improve the GB model by inserting nanoscaled voids (nanovoids) within them. This is the first time that such simulations are achieved. We demonstrate here

that such nanoscale defects have a profound impact on the interfacial shear strength and underlying deformation mechanisms in copper GBs due to void-induced local stresses. We emphasize three kinds of dependencies whether the involded nanomechanisms are GB-mediated dislocation emission, interface sliding or shear-coupled GB migration. For all GB types, the interfacial shear strength is shown to decrease linearly as the volume fraction of voids at the interface increases. In addition, owing to larger void-induced stresses, this decrease is found to be much more pronounced in the GBs deformed by shuffling than by other mechanisms. This last study constitutes a first step aimed at improving the predictions of the two-scale model.

In sum, this thesis introduces the following novelties:

- Development of an atomistically-informed two-scale model: We enhanced the FEM proposed in Ref. [39] by fully calibrating the GBs. To this end, the research of the parameters of GBs undergoing tensile and shear loadings using QC has been automated and a GB decohesion model has been added in the DNS framework. The CRSS of the plasticity model presented in Ref. [11] has been calibrated using a QC nanoindentation model accounting for dislocation-GB interactions and grain sizes.

- Development of a fully-atomistic QC model of a large polycrystalline RVE with a view to validating the two-scale model.

- Adaptation of the two-scale model for larger problems: To this end, a simplified GB calibration adapted to HA-type textures has allowed to perform large ($> 100$ grains) and atomistically-informed NCs simulations accounting for both the grain size and texture.

- Study of defective GBs with a view to enhancing the two-scale model: A defective GB model with QC has been developed and allowed for the development of a void-induced stress model.

This thesis is based on the compilation of two published papers [64, 66] and on a paper [65] currently under review. These three papers are attached in Appendix A, C and B, respectively, and are summarized in the following three chapters.

# Chapter 2

# A two-scale model predicting the mechanical behavior of nanocrystalline solids

In this first Chapter, the numerical multiscale model is presented. The aim of this model is to predict the mechanical behavior of NC metals/solids by taking into account their specific crystallography or GBCDs, without suffering from the length scale limitations encountered when dealing with atomistic simulations. To this end, the constitutive equations of both constitutive elements (grains and GBs) are exposed. The calibration of these models are then achieved by recourse to QC through GBs and nanoindentation simulations. Finally, the application of the method on a 16-grain and 34-GB RVE is presented for two GBCDs.

## 2.1 Grain constitutive model

In this framework, grains are discretized with a fine mesh and the elasto-plastic formulation described in Ref. [45] for the FCC polycrystal is used to address the forest dislocation-based hardening model of grains. The following power-law is used to describe the shear rate deformation of each slip system $\alpha$

$$\dot{\gamma}^{\alpha} = \begin{cases} \dot{\gamma}_0 \left[ \left( \frac{\tau^{\alpha}}{g^{\alpha}} \right)^{\frac{1}{m}} - 1 \right], & \text{if } \tau^{\alpha} \geq 0 \\ 0, & \text{otherwise} \end{cases} \tag{2.1}$$

where $\dot{\gamma}_0$ is the reference shear strain rate, $m$ the strain-rate sensitivity exponent, and where $g^{\alpha}$ and $\tau^{\alpha}$ are the critical resolved shear stress (CRSS) and the resolved shear stress on slip system $\alpha$, respectively. Based on statistical mechanics [61], the evolution of the flow stresses in the case of multiple slip systems is governed by a diagonal hardening

law

$$\dot{g}^{\alpha} = \sum_{\beta} h^{\alpha\beta} \dot{\gamma}^{\beta} \tag{2.2}$$

where $h^{\alpha\beta}$ are the diagonal hardening moduli. This formulation, based on the activation of slip planes, allows for the intragranular plasticity to occur when one of these slip planes $\alpha$ reaches a critical value called critical resolved shear stress (CRSS), $g^{\alpha}$. In this hardening model, the initial value (i.e. before hardening) of $g^{\alpha}$ is $g_0$. The originality of our method consists in calibrating this value with the QC method by means of nanoindentation tests, see Figure 2.1. In these QC simulations, a rigid rectangular indenter

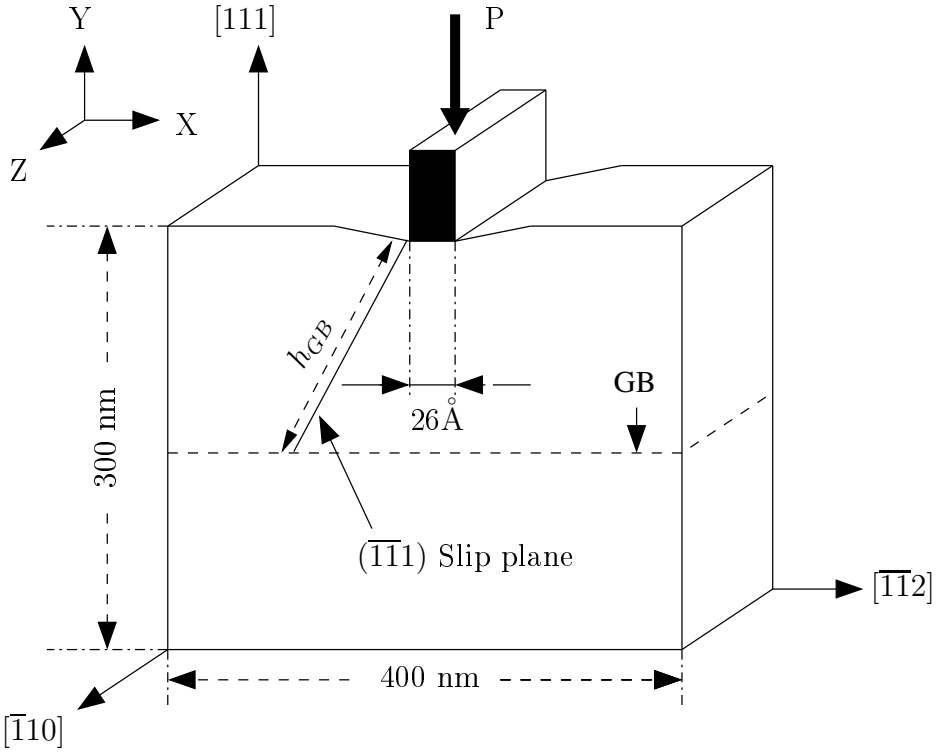


Figure 2.1: Schematic representation of the nanoindentation model with a GB.

is driven into a thin copper film. $g_0$ is taken as being the maximum stress measured before a partial dislocation emission from the indented surface. A grain size effect is added in the QC model by inserting different GB kinds (HA or LA) in the direction of the propagation of the partial dislocation. These GBs are supposed to empede, or not, the motion of the incipient dislocation. It is worth noting that the QC method does not offer the possibility to compute the atomic stress in the non-local zone, i.e. in the atomistic zone. This poses a problem since it is precisely in this zone that the dislocation motion appears and that $g_0$ must be computed. To overcome this problem, we have developed an algorithm allowing for the virial stress to be computed according to the atomic positions, as it was already developed in Ref. [89]. The computation of

the virial stress is based on the virial theorem exposed by Clausius and Maxwell in 1870 and is generally not considered as a relevant computation of the atomic stress due to the difficulties encountered when trying to evaluate the atomic volume in a deformed configuration. To address this issue, a voronoï 3D tesselation built with the voro++ library available on the internet, allowed us to compute the volume occupied by each atom and therefore, resulting in a virial stress presenting all mechanical stress characteristics. Eventually, for both GB kinds, $g_0$ increases when the grain size is decreased, highlighting the empediment to the motion of the dislocation for small grain sizes, as shown in Figure 2.2.

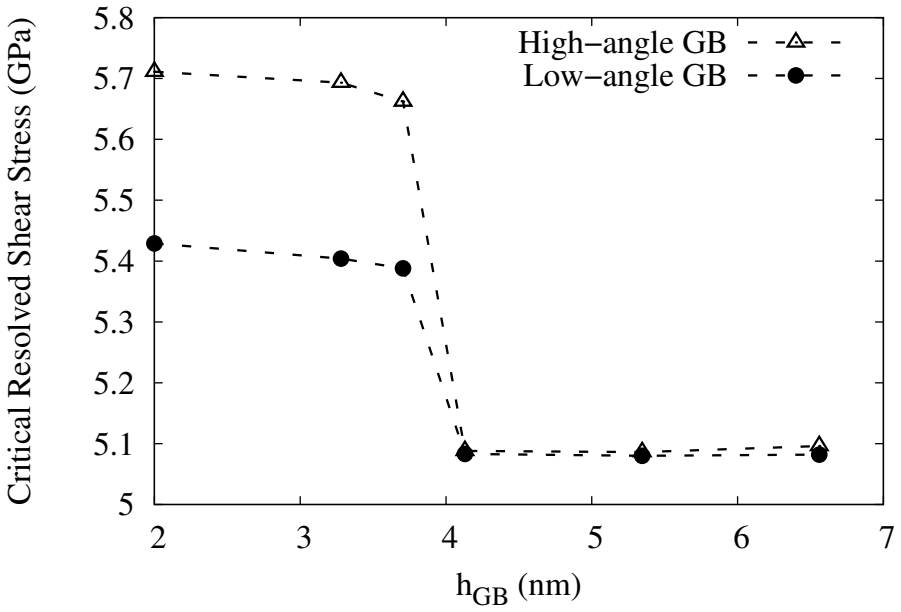


Figure 2.2: Initial CRSS ($g_0$) evolution with $h_{GB}$ for HA and LA GBs.

## 2.2 Grain-boundary constitutive model

In the FEM model, GBs are surfaces of discontinuities embedded in the continuum, see Figure 2.3. The local stress state is described by the Cauchy stress tensor $\underline{\underline{\boldsymbol{\sigma}}}$ whereas local information about the material deformation is conveyed by the deformation gradient field $\underline{\underline{\boldsymbol{\epsilon}}}$. The material model required to evaluate $\underline{\underline{\boldsymbol{\sigma}}}$ in the bulk as well as the surface traction $\underline{\underline{\boldsymbol{t}}}$ at the GBs are defined below. The mean deformation mapping is defined as set in Ref. [60]

$$\underline{\tilde{\varphi}} = \frac{1}{2}(\underline{\varphi}^{+} + \underline{\varphi}^{-}) \tag{2.3}$$

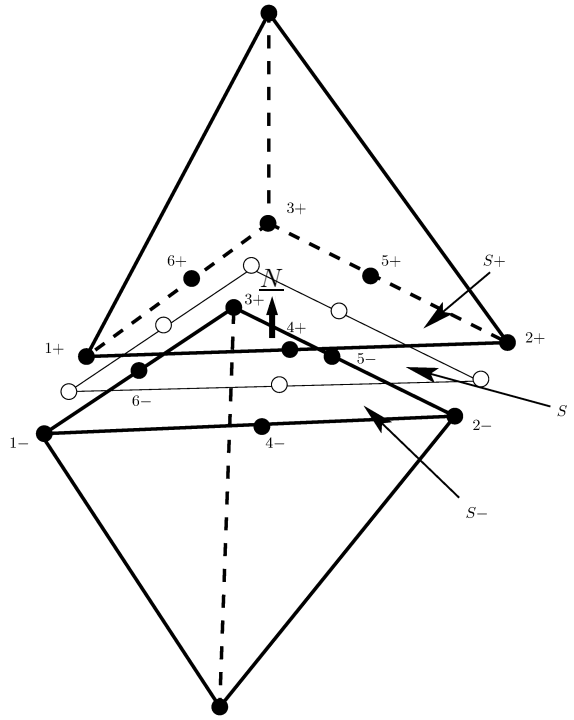


Figure 2.3: Schematics of a GB element. Two tetrahedra belonging to two adjacent crystals separated by an interface element at the GB: $S+$ and $S-$ are respectively the facets corresponding to the tetrahedra on the positive and negative sides, as defined by the positive surface normal $\underline{\boldsymbol{N}}$, and $S$ is the midsurface.

By using Equation (2.3) we recover the original deformation mapping on both sides of the GB

$$\underline{\boldsymbol{\varphi}}^{\pm} = \underline{\tilde{\boldsymbol{\varphi}}} \pm \frac{1}{2}(\underline{\boldsymbol{\varphi}}^{+} - \underline{\boldsymbol{\varphi}}^{-}) = \underline{\tilde{\boldsymbol{\varphi}}} \pm \frac{1}{2}\underline{\boldsymbol{\delta}} \tag{2.4}$$

where

$$\underline{\boldsymbol{\delta}} = [\![\underline{\boldsymbol{\varphi}}]\!] = \underline{\boldsymbol{\varphi}}^{+} - \underline{\boldsymbol{\varphi}}^{-} \tag{2.5}$$

is the displacement jump at the GB that can be decomposed into a GB opening vector and a sliding vector as follows

$$\underline{\boldsymbol{\delta}}_n = (\underline{\boldsymbol{\delta}} \cdot \underline{\boldsymbol{N}})\underline{\boldsymbol{N}} = (\underline{\boldsymbol{N}} \otimes \underline{\boldsymbol{N}}) \cdot \underline{\boldsymbol{\delta}} \tag{2.6}$$

$$\underline{\boldsymbol{\delta}}_s = \underline{\boldsymbol{\delta}} - \underline{\boldsymbol{\delta}}_n = (\underline{\underline{\boldsymbol{I}}} - \underline{\boldsymbol{N}} \otimes \underline{\boldsymbol{N}}) \cdot \underline{\boldsymbol{\delta}} \tag{2.7}$$

This kinematics imposes a constant state of deformation across the thickness $h$ of the GB, which can be expressed in the local orthonormal reference frame $(\underline{\boldsymbol{N}}_1, \underline{\boldsymbol{N}}_2, \underline{\boldsymbol{N}})$, where $\underline{\boldsymbol{N}}_1$ and $\underline{\boldsymbol{N}}_2$ are the two local tangents. Thus the strain can be written as

$$\underline{\underline{\boldsymbol{\epsilon}}} = \underbrace{\frac{\underline{\boldsymbol{\delta}}_n \cdot \underline{\boldsymbol{N}}}{h} \underline{\boldsymbol{N}} \otimes \underline{\boldsymbol{N}}}_{\underline{\underline{\boldsymbol{\epsilon_n}}}} + \underbrace{\frac{\underline{\boldsymbol{\delta}}_s \cdot \underline{\boldsymbol{N}}_1}{h} \frac{1}{2}(\underline{\boldsymbol{N}}_1 \otimes \underline{\boldsymbol{N}} + \underline{\boldsymbol{N}} \otimes \underline{\boldsymbol{N}}_1) + \frac{\underline{\boldsymbol{\delta}}_s \cdot \underline{\boldsymbol{N}}_2}{h} \frac{1}{2}(\underline{\boldsymbol{N}}_2 \otimes \underline{\boldsymbol{N}} + \underline{\boldsymbol{N}} \otimes \underline{\boldsymbol{N}}_2)}_{\underline{\underline{\boldsymbol{\epsilon_s}}}}$$

As shown in this latter equation, $\underline{\underline{\boldsymbol{\epsilon}}}$ can be seen as the sum of two quantities; a normal opening part $\underline{\underline{\boldsymbol{\epsilon_n}}}$ and a sliding part $\underline{\underline{\boldsymbol{\epsilon_s}}}$. $h$ naturally introduces a characteristic length scale of GBs in the model and is set to 1 nm following past works [94, 48]. This setting of $h$ concerns only the first part of this thesis. The next study, presented in Section 3, includes some special considerations on the GB width treatment. The traction is eventually expressed as

$$\underline{\bar{\boldsymbol{t}}} = h\underline{\underline{\boldsymbol{\sigma}}} : \frac{\partial \underline{\underline{\boldsymbol{\epsilon}}}}{\partial \underline{\boldsymbol{\delta}}} = \underline{\underline{\boldsymbol{\sigma}}} \cdot \underline{\boldsymbol{N}} \tag{2.8}$$

Only the sliding component undergoes plastic deformations and a damage parameter $D$ is included in the GB opening mechanical behavior. The elasto-plastic model described in Ref. [39] is used to compute the sliding part $\overline{\underline{\boldsymbol{\sigma}}}^{\boldsymbol{sl}}$ of the effective stress tensor and is characterized by the yield stress tensor $\sigma_p$ with

$$\sigma_p = \sigma_0(1 + \frac{\bar{\epsilon_p}}{\epsilon_0}) \tag{2.9}$$

where $\bar{\epsilon}_p$ is the equivalent plastic strain, $\sigma_0$ is the initial yield stress, and $\epsilon_0$ is the reference plastic strain. The damage parameter $D$ is evaluated from the normal opening $\underline{\boldsymbol{\delta}}_n \cdot \underline{\boldsymbol{N}}$. While this opening remains relatively small, the opening stress $\overline{\underline{\boldsymbol{\sigma}}}^{\boldsymbol{op}}$ remains smaller in norm than the critical stress $\sigma_c$ and $D = 0$. Once $\sigma_c$ is reached, $D$ increases in an irreversible way, and eventually reaches 1 for a critical opening $\delta_c$. Finally the stress tensor is directly computed from

$$\underline{\underline{\boldsymbol{\sigma}}} = (1 - D)(\overline{\underline{\boldsymbol{\sigma}}}^{\boldsymbol{sl}} + \overline{\underline{\boldsymbol{\sigma}}}^{\boldsymbol{op}}) \tag{2.10}$$

Because the constitutive behavior of one GB is based here on its ability to slide or open, the sliding and the opening behaviors are calibrated by shearing or by applying tensile loading to bicrystals designed with QC. Based on past QC studies, see Ref. [79, 80], the QC simulations achieved here account for the specific crystallography of each GB, see Figure 2.4. The shear modulus $G$, the yield stress $\sigma_0$, the critical stress $\sigma_c$ and the strain-to-failure $\delta_c$ are extracted from QC results and are used as inputs for the FEM.

These QC simulations enabled us to assert that $\sigma_c$ and $\delta_c$ are higher in LABs than in HABs, giving new interesting insights on the specific natures of the GBs involved. This work demonstrates that a unique arbitrary law is not enough to capture the special nature of each GB, unlike the prevailing assumption made in past studies.

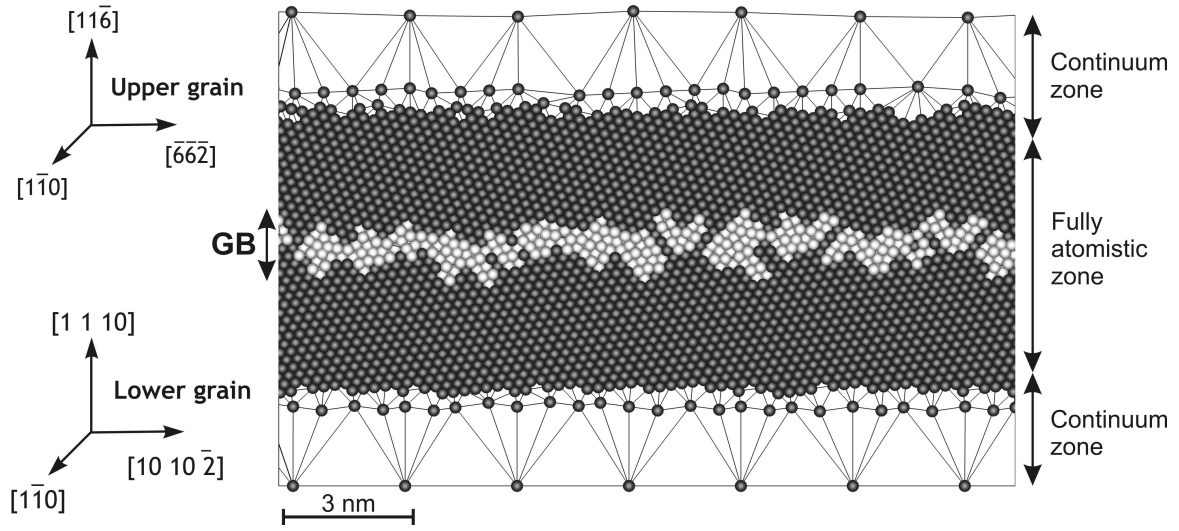


Figure 2.4: Quasicontinuum model of $GB_{10-7}$ in the HA texture. The continuum and the atomistic regions are indicated. The crystals orientation and GB position after relaxation are also shown. Atoms appearing in dark color present a perfect FCC stacking. Bright-colored atoms correspond to crystal defects.

## 2.3 Two-scale numerical simulations

The two-scale model is aimed at predicting the mechanical behavior of NC solids and is calibrated in this work for copper in the case of two textures (HA and LA) and for two average grain sizes. Overall, with the RVE chosen consisting of 16 grains and 34 GBs, see Figure 2.5, 136 QC simulations (GB sliding, GB decohesion, interaction GB-dislocation) are required to fully calibrate the two-scale model to study two different textures and two different average grain sizes. The grain sizes and the textures have been chosen in order to illustrate the ability of the model to capture the RHP effect and its dependency on the texture considered.

Three kinds of calibration are considered to highlight the relative importance of the GB nature proportion in the deformation process. In the first model (set 1), grains are elastic, GB sliding is calibrated and GB decohesion is not taken into account. In the second one (set 2), grains are elastic and both GB sliding and opening are set. In the third set (set 3), intragranular plasticity is calibrated as well as GB sliding and GB decohesion. Tensile loading is applied for every set of simulations on the LA- and HA-type textured RVEs for different grain sizes. For every set of parameters, the same elastic behavior is observed and discrepancies appear with the plastic behavior. The resulting yield stresses decrease when going from set 1 to 3. In fact, the higher the number of constitutive mechanical laws inducing plasticity in the model, the earlier the plasticity. This demonstrates the need to consider an accurate constitutive behavior of both grains and GBs. A reduced material strength is also observed when the grain size decreases. The model shows here its ability to capture precisely the RHP effect predicted by atom-

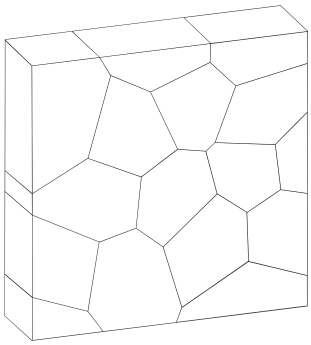

Figure 2.5: RVE consisting of 16 grains.

istic simulations. The LA textures are found to present longer elastic deformations and higher yield stresses than their HA counterparts. Because LABs present higher yield stresses, LA texture simulations allow for the competition between intragranular and intergranular plasticity to be captured. Conversely, HABs slip more easily due to their lower yield stresses and this makes difficult the identification of the activation of the intragranular plasticity in HA textures. Consequently, for such small grains, the model confirms the importance of taking into account the specific nature of the GB network to properly predict the NC behaviors.

The results are compared to MD results extracted from Ref. [84] and are found to be overvalued. This lies in the 2D nature of QC used for the calibration process and also because no thermally activated process is taken into account here. Nevertheless, even if some improvements are required to capture a good quantitative response, the model remains qualitatively efficient. Such a model opens the way to simulation frameworks able to automatically characterize GBs behaviors as a function of intergranular evolutions, while not necessarily fully modeling them. Such feature could be of crucial importance in the simulation of a recently discovered substitute for nanocrystals, namely nanotwinned ultrafine crystals.

The related article is given in Appendix A.

# Chapter 3

# Two-scale computational modeling of intergranular fracture in nanocrystalline copper.

This second part, taking the form of a paper submitted to the Computational Materials Journal, see Appendix B, is a direct continuation of the first Chapter [64]. In this study, the GB thickness $h$ was arbitrarily set to 1 nm, following the previous studies addressing the GB thickness issue, see Ref. [94, 48]. Thus a finer GB calibration is achieved in this work through a more accurate determination of the GBs thicknesses. Then, the two-scale model is compared to a fully-atomistic QC model in order to validate it numerically. Finally, based on the trends of the GBs parameters presented in Ref. [64], a fitting process is presented in order to easily calibrate HA-type textured structures consisting of a large number of grains. This work also focuses on the ability of the model to predict the evolution of the intergranular fracture in NC metals.

## 3.1 GB width calibration

A more detailed observation of the GBs reveals that the widths of GBs are different depending on the nature of the GB considered. Based on a threshold of 0.1 for the centrosymmetry parameter $p$ [40], helping measuring the degree of crystallinity of the FCC crystal lattice, the widths of GBs are determined for all the GBs involved in the previous Chapter. This GB thickness study allows for the identification of trends when considering GB thicknesses as a function of the GB misorientations. In order to test the sensitivity of the two-scale model to the GB width, tensile tests are performed on LA- and HA-type textured RVEs while averaging their GBs widths to 0.8 nm and 1.5 nm, respectively. The RVE used for this study is the same that was used in the previous Chapter.

It is found that averaging HAB widths in the HA-type textured RVE does not result in any significant change in the RVE behavior. Conversely, in the LA case, this averaging

leads to different behaviors concerning the propagation of the intergranular crack. In fact, due to the high variability observed in the case of the LA parameters, no fitting process seems to be appropriate to allow for the LA-type RVE behavior to be properly captured. However, in the HA case, trends are clear and not subjected to high variations. There, we apply a fitting process, as shown in Figure 3.1, that enables the obtention of the GB parameters according to their misorientations without having to compute all the GB simulations. In Figure 3.1(f), the initial CRSS $g_0$ of FCC slip systems as a function of the pseudo grain size $h_{GB}$ as extracted from nanoindentation tests [64] is also reproduced to gather all the parameters required for NC simulations.

## 3.2 Numerical validation

The numerical validation of the two-scale model is then performed by comparing its predictions with a fully-atomistic model. To this end, we fully calibrate the two-scale model, meaning that $\sigma_0$, $G$, $\sigma_c$, $\delta_c$, $h$, $g_0$ are all calibrated from QC simulations (not from fitting process). The model validation is based on simulations addressing the behavior of 4 RVEs, LA- and HA-types, for two mean grain sizes. This model is illustrated in Figure 3.2 showing one HA-type texture presenting a mean grain size of 6.56 nm. It must be emphasized that performing fully-atomistic simulations with QC while properly relaxing the GBs is problematic because of the mixed nature (atomistic-continuum) of QC. These problems have been solved in the framework of this thesis and this must be seen as a novelty.

Then, we apply the same loading conditions for both models (two-scale and fully-atomistic) and the stress-strain curves as well as the deformed configurations are compared. The weak points of the GB networks are found to be the same in both models. Moreover, the paths followed by the intergranular cracks are quite similar, whatever the mean grain size or the nature of the GB networks. The stress-strain curves analysis reveals that both models predict the same trends concerning the texture yield stresses when decreasing the grain size, also called RHP effect. However, the two-scale model is found to be more rigid than the fully-atomistic model. This higher stiffness is believed to originate from the absence of triple junction calibration in the two-scale model.

## 3.3 Dogbone study

As a last step, and in order to illustrate the ability of the two-scale method to deal with larger problems, we study the mechanical response of a HA-type dogbone consisting of 103 grains and 251 GBs, see Figure 3.3. The calibration of the GBs $(\sigma_0, G, \sigma_c, \delta_c, h)$ of the whole GB network is done by using the fitting process previously exposed. This study allows for the observation of the transition from an intergranular to an intragranular driven plasticity for small grain sizes. This highlights the crucial role played by both constitutive elements (grains and GBs) when grains are that small. This method is

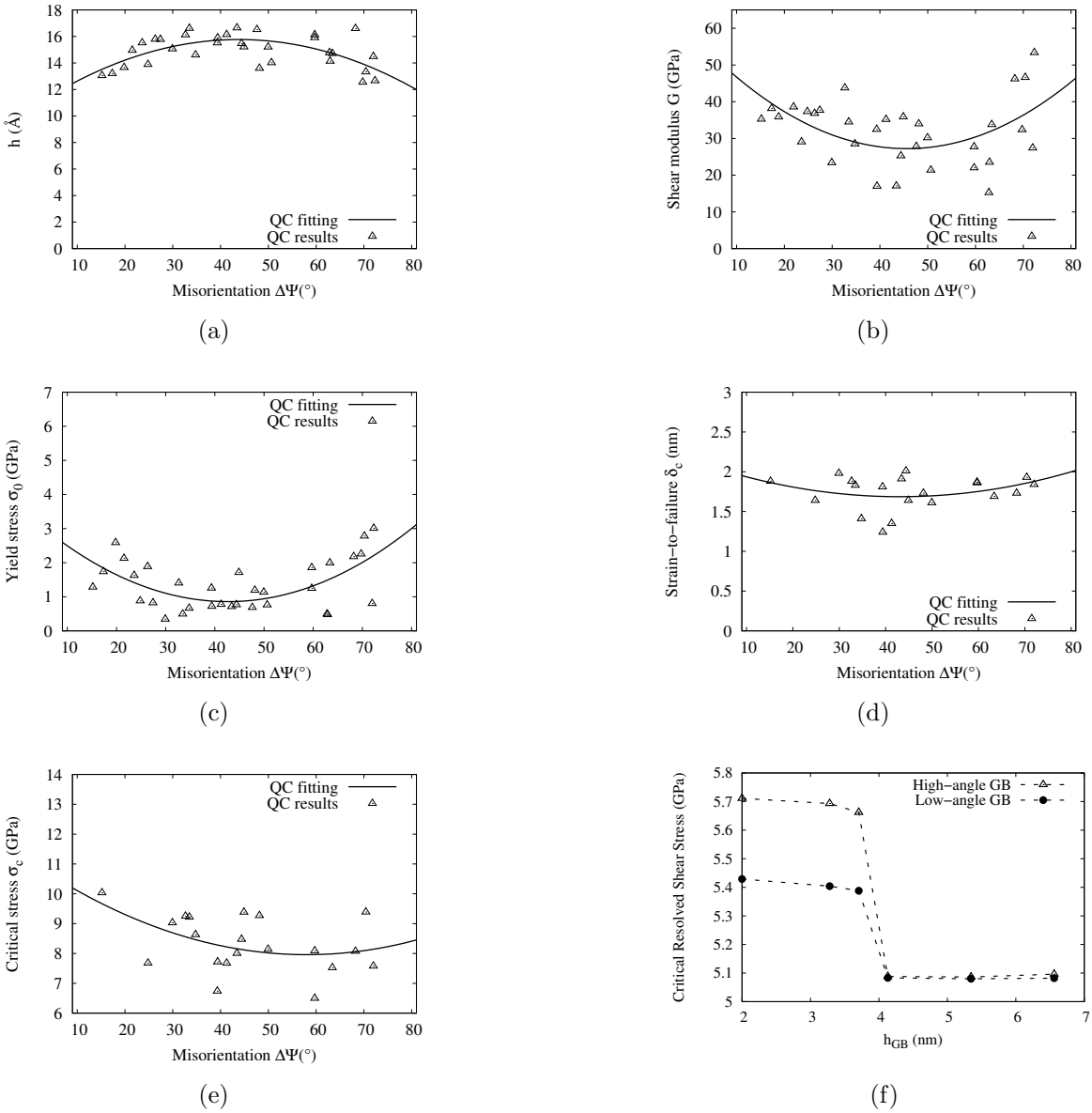


Figure 3.1: Fitting of GB parameters: a) $h$, b) $G$, c) $\sigma_0$, d) $\delta_c$, e) $\sigma_c$. f) CRSS ($g_0$) evolution with $h_{GB}$ for HA and LA GBs.

adaptable to other tilt axes and opens the door to an exciting new approach to predict columnar thin film behaviors regardless of the number of grains consisting the sample.

To conclude, this part gives for the first time more accurate insights on the widths of the $[1, \overline{1}, 0]$ tilt GBs. It also reveals the sensitivity to the calibration process when dealing with LA-type textures or the possible fitting when addressing HA-type textures (fitting possible). Finally, this work highlights the importance of taking triple junctions into account in the two-scale framework. The calibration of such special elements of

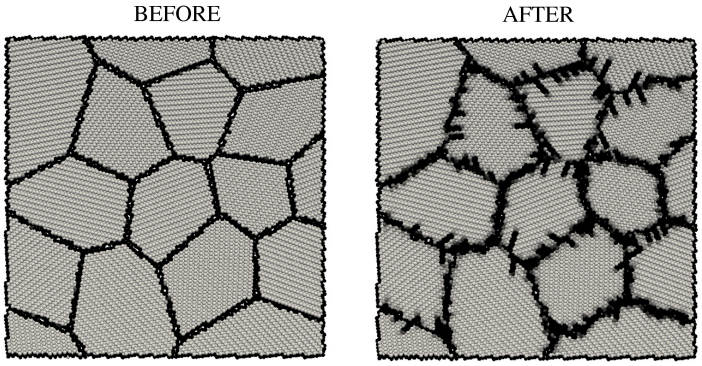


Figure 3.2: Fully-atomistic model in the case of the HA-type texture with a mean grain size of 6.56 nm, before and after relaxation step.

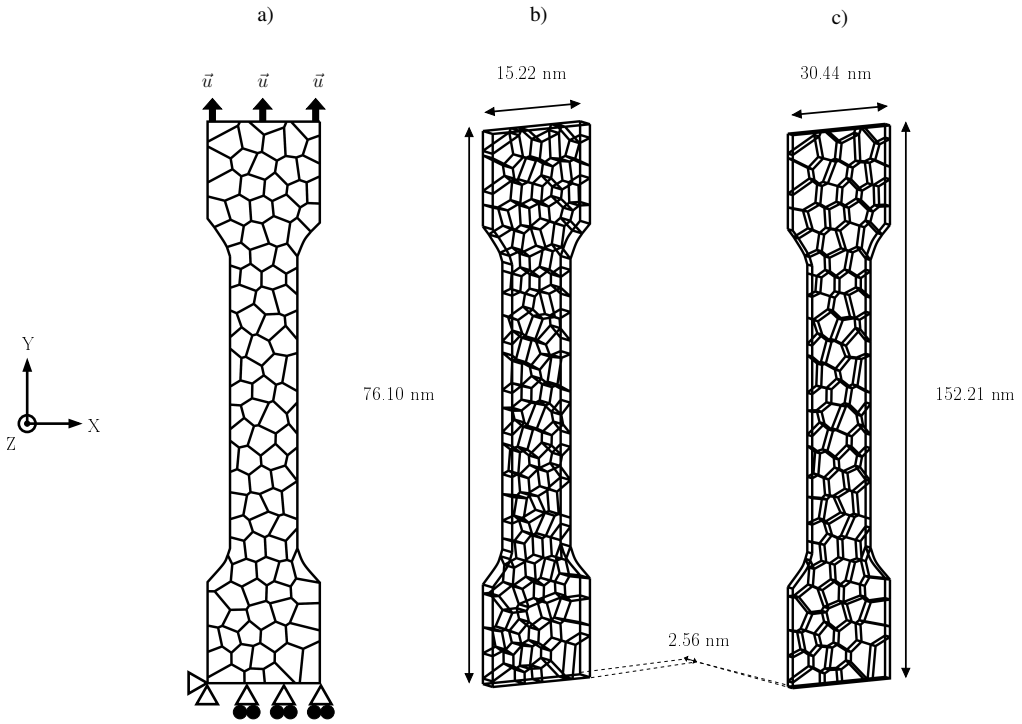


Figure 3.3: Boundary conditions and dogbone dimensions. a) Tensile loading boundary conditions. Nodes are fixed in the Z directions. Dimensions of dogbones with a grain size set to b) 3.28 nm and c) 6.56 nm.

the GB networks would help to reduce the overvaluation of the model in comparison to experiments and MD. This overvaluation lies also in the fact that no defects and thermally activated processes are accounted for in the model.

# Chapter 4

# Quasicontinuum study of the shear behavior of defective tilt grain boundaries in Cu

As we have seen in the two previous studies, the two-scale model results provided in the framework of this thesis are overvalued comparatively to the ones observed in fully-atomistic models whether statics (QC) or dynamics (MD), or more generally compared to experiments. In particular, the overvaluation concerning the GB yield stresses is partly due to the fact that the GBs do not include any defects, kinks or nano-scaled voids (nanovoids). The 2D nature of QC and the fact that our simulations do not take into account any thermally activated process also help to rationalize this overvaluation. In order to improve the two-scale model presented in Ref. [64,65], we choose as a first step to focus on the insertion of nanovoids within the GBs in hopes of identifying mechanical behaviors closer to reality.

## 4.1 Methodology

It has been shown that in pure tension, growth and coalescence of nanovoids smaller than a few nanometers in diameter can participate collectively in shear band formation and localized plastic deformation processes that result in significant material softening of metals [51, 16, 50, 77]. These nanovoids, present in metals, have been studied using MD technique and mixed atomistic/finite-element simulations [88, 73, 107, 109]. MD studies have focused on the dislocation dynamics in growth and coalescence of voids in single crystals [7]. In Ref. [25], interstitial atoms or vacancies were added inside GBs and showed multiple phases with different atomic structures. However, this latter study did not specifically address the impact of vacancies on the deformation processes and on the mechanical response of GBs. NC GBs have been predicted to exibit characteristic deformation processes. There are three of these: GB-mediated dislocation emission (process 1) [98, 46, 83, 81], interface sliding (process 2) [82, 98, 97, 78, 17, 81] and shear-

coupled GB migration (process 3) [76, 5, 28, 49, 74, 17]. In the process 1, the plastic flow under mechanical loading is accommodated by dislocation emission from the periodic defects of the GB. In the second process, the accomodation is due to atomic shuffling, i.e. by inhomogeneous displacements of an array of atoms in the layers immediately adjacent to the GB. Finally, in the third process, shear-coupled GB migration corresponds to a deformation process for which the crystalline interface is displaced in the direction perpendicular to the GB plane when subjected to pure shear loading along its tangential direction. Thus the aim of this study is to determine the influence of nanovoids on the deformation processes cited above. Five tilt bicrystals containing GBs are chosen as witnesses of these three processes. These GBs are submitted to shear tests with QC, as in Ref. [79, 80], while varying the void volume concentration inside them. Process 1 is represented by one HAB and one LAB. Process 2 corresponds to $\Sigma 9(221)$. Finally, process 3 is studied through $\Sigma 27(115)$ and $\Sigma 5(210)$ GBs.

To this end, the model presented in Ref. [79, 80] is implemented in order to allow for the insertion of nanovoids in GBs. This implementation offers the possibility to vary the number and the diameter of the nanovoids inserted, which is the same as varying the void volume concentration in the GBs. The QC modeling is illustrated in Figure 4.1.

## 4.2 Results

The interfacial shear strengths experienced at the yield point by the bicrystals undergoing shearing are extracted from these defective GBs simulations, as it can be seen for perfect tilt GBs in Figure 4.2. We show that for all GBs, the interfacial shear strength decreases as the void volume fraction at the interface increases, see Figure 4.3. Different deformation nanomechanisms depending upon the number and size of the nanovoids, and upon the process involved, are found compared to the case of non-defective GBs. For process 1, i.e. in the GB-mediated dislocation emission case, dislocations are found to be preferentially emitted from voids, instead of intrinsic GB sites; more so in the LAB interface than in the HAB interface. Also, nanovoids are found to act as pinning points that impede atom shuffling across the interfaces for the process 2. In the case of the third process, the effect of nanovoids on shear-coupled migration is found to depend on the GB type. In the $\Sigma 5(210)$ GB, migration is not significantly affected and no dislocation emission is observed. On the contrary, $\Sigma 27(115)$ GB undergoes significant perturbations in its migration and preferentially emits dislocations when voids become larger.

## 4.3 Model

We then develop a model aiming at describing the decrease of the interfacial shear strength $\sigma_{max}$ as a function the void volume concentration $V$. The proposed expression

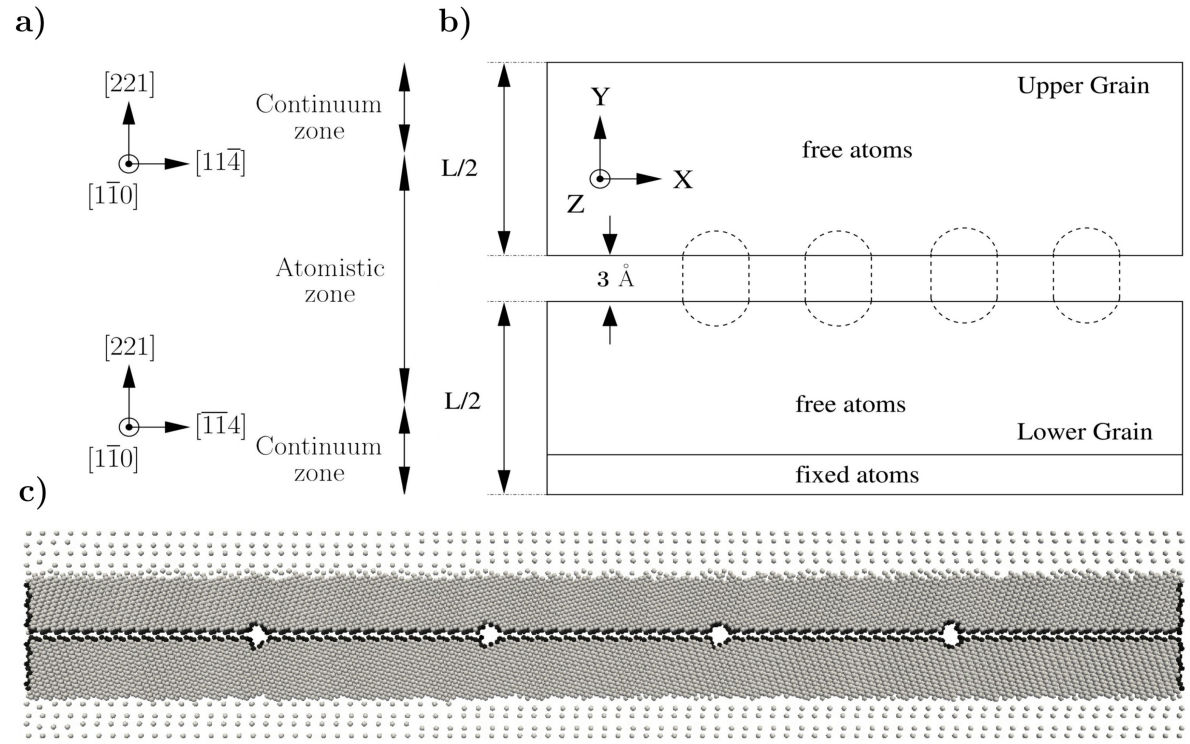


Figure 4.1: Quasicontinuum modeling of a tilt bicrystals containing nanovoid defects at the interface. a) Schematics of atomistic and continuum zones, and crystal orientations for a Σ9(221) GB. b) Boundary conditions for zero force lattice relaxation used to simulate 0 K equilibrium GB structures. Voids are represented with dashed lines. c) Atomistic snapshot before relaxation for a Σ9(221) GB in Cu with a void volume fraction equal to 1.48% (4 voids, diameter 10 Å). Bright-colored atoms are in perfect FCC crystal lattice (zero centrosymmetry). Dark-colored atoms are part of crystal defects (non-zero centrosymmetry).

takes the following form

$$\sigma_{max} = (1 - V) * \sigma_{max_0} + V * \sigma_v \tag{4.1}$$

where $\sigma_{max_0}$ is the interfacial shear strength when no nanovoid is present (perfect GB). The missing parameter, $\sigma_v$, is a residual stress acting in the vicinity of the defect and is evaluated by rewriting equation (4.1) in

$$\frac{\sigma_{max}}{\sigma_{max_0}} = 1 - V * (1 - \frac{\sigma_v}{\sigma_{max_0}}) \tag{4.2}$$

so that the results for each GB can be represented as in the Figure 4.3 which shows the slope for each GB and highlights the relative values of $\sigma_v$. According to the model,

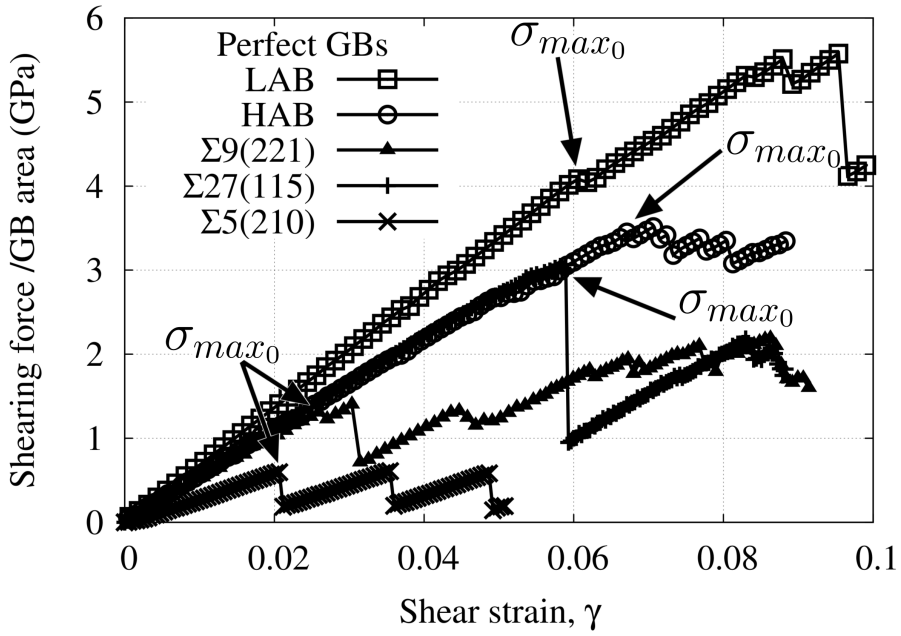


Figure 4.2: Shear stress *vs.* $\gamma$ curves for different GBs (LAB, HAB, Σ9(221), Σ27(115), Σ5(210)) in Cu in the absence of voids. $\sigma_{max_0}$ is the maximum stress reached by all GBs without voids at the plastic deformation onset.

represented by Equation (4.2), $\sigma_v$ is found to be negative, i.e. found to be responsible for a shield effect to the applied stress. In order to illustrate this finding, the virial stresses at the atomic level are computed. The ruling stresses analysis in the vinicity of the nanovoids reveals a perfect correlation between the virial stresses and the $\sigma_v$ values shown in Figure 4.4. This result confirms the existence of a stress concentration in the nanovoids vicinity, acting against the applied stress, and showing different values depending on the nature of the process (1, 2 or 3) involved.

The model presented here is a first step in understanding the effect of nanovoids defects on the GBs of NCs. It is now possible to determine the laws ruling the yield stress decrease as a function of the void volume concentration when the process involved is established. This model, although not yet used in the two-scale framework, will allow for the reduction of the overvaluation encountered while using the atomistic simulation calibration.

The corresponding study, published in Acta Materialia, is reproduced in Appendix C.

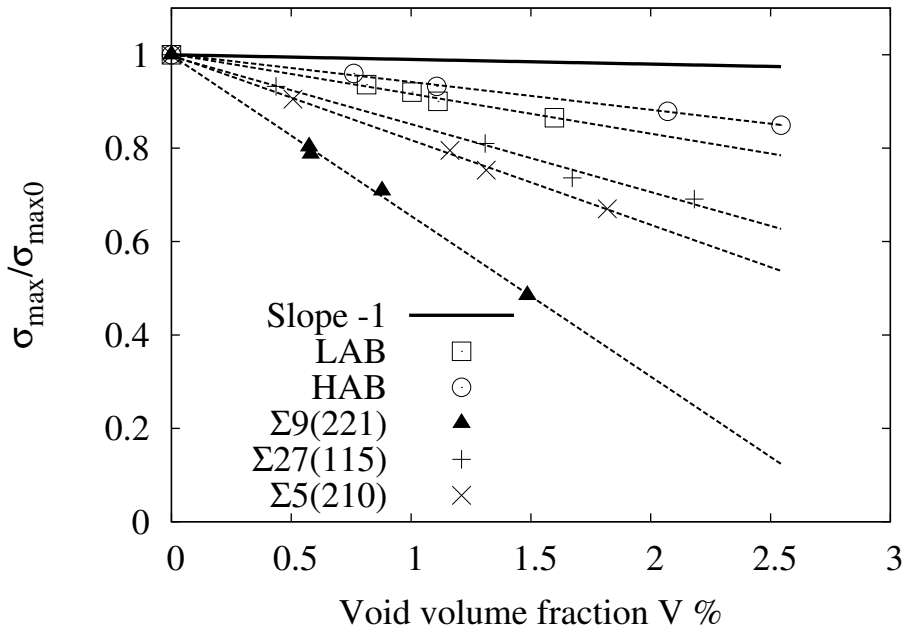


Figure 4.3: Fitting of $\sigma_{max}/\sigma_{max_0}$ *vs.* void volume fraction $V$ by equation (4.2) (dashed lines). The model predictions with no void-induced stress ($\sigma_v = 0$) are shown with a solid line for comparison.

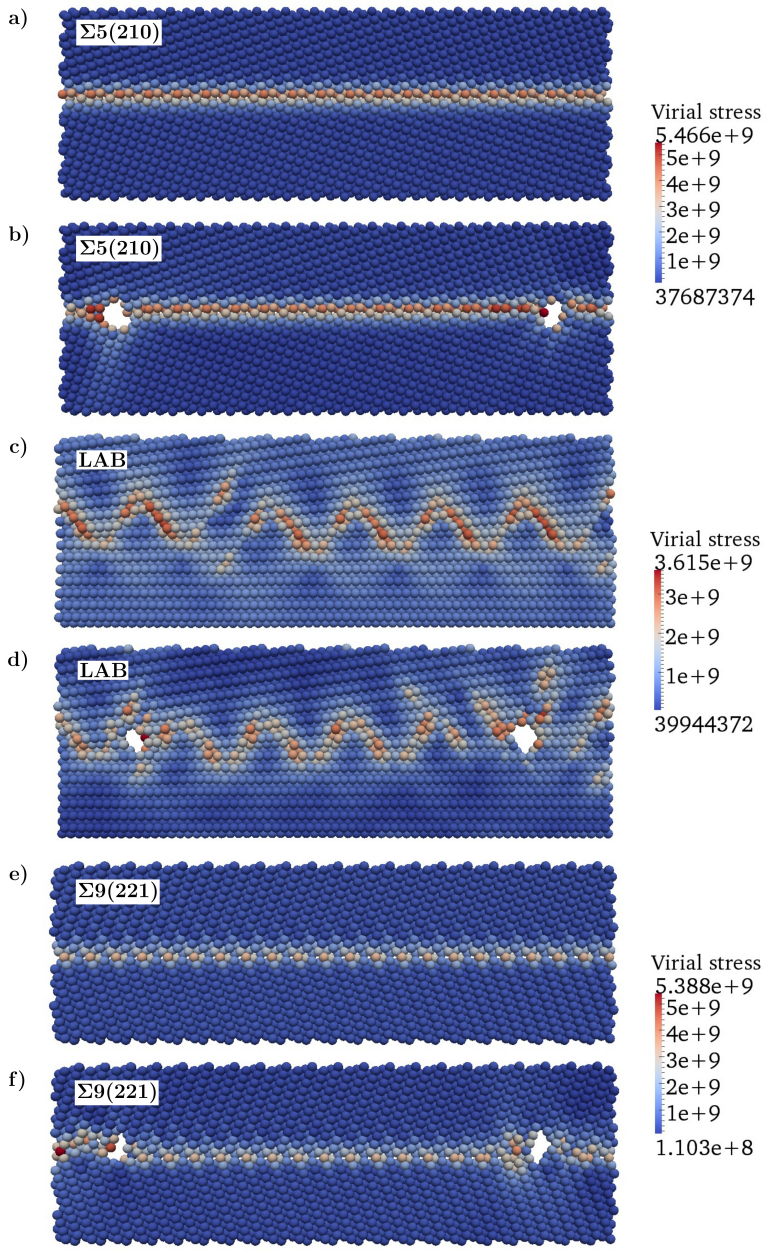


Figure 4.4: Virial stress (von Mises) (Pa) snapshots (partial views of the GBs) before yield point when a) no void and b) voids are inserted in a Σ5(210) GB. c) and d) same analysis for a LAB interface. e) and f) ditto for a Σ9(221) GB.

# Chapter 5

# Conclusions

The aim of this thesis was to develop a two-scale numerical model, atomistically-informed, able to predict the mechanical behavior of NC metals as a function of their particular crystallography. Generally adaptable to FCC and BCC solids and enhancing the understanding of NCs, this method does not suffer from length-scale limitations conventionally encountered when studying NCs with atomistic methods. The challenge taken up in the framework of this thesis has been to numerically calibrate the material laws governing the constitutive elements, grains and GBs, from QC atomistic simulations.

Laws governing the GB sliding and GB opening were based on QC simulations of oriented bicrystals undergoing shear and tensile loadings, respectively. In addition, these simulations provided the trends of the HABs parameters allowing for an easier calibration of the HA-type textures, through a fitting process as a function of the misorientation. Conversely, these GB simulations highlighted the difficulties faced when dealing with LABs. In this last case, LABs parameters are subjected to large variations when considering them as a function of their misorientations, making the fitting process impossible.

The grains behaviors were described by a forest dislocation hardening model that has been calibrated using nanoindentation QC simulations. The determination of the initial critical resolved shear stresses resulting from QC simulations allowed to highlight not only the grain-size effect, but also its dependency with the nature of the texture considered.

The QC calibration of the constitutive elements of the FEM has allowed us to capture the competition taking place between intragranular and intergranular plasticity behaviors in NCs metals, depending on the grain size considered giving rise in particular to the RHP effect. In this way, the model demonstrated its ability to predict the NCs behaviors when varying the mean grain size and/or the GBCD. Moreover, the model was able to predict not only the GB networks weak points but also the direction of the intergranular crack propagation. We have also noted however that taking triple junctions into account is a possible way to improve the ability of the model to predict the crack propagation direction.

Based on the trends of the GBs parameters fully characterized using QC, a fitting process was presented in order to simplify the HA-type texture calibration, allowing for the simulations of samples consisting of a substantial number of grains and avoiding the need for extra QC simulations.

Finally, the absence of GBs defects in the GB simulations led to results quantitatively overvalued compared to experiments and fully-atomistic models. To solve this problem, an original study has been carried out on the insertion of nanovoids in the GB simulations. This study showed that the introduction of nanovoids in GBs subjected to shear loading results in a significant GB softening leading to a linear decrease of the yield strength with respect to the void volume fraction. This decrease has been found to depend on the deformation mechanism involved in the defective GB. This last study must be seen as a first step toward the improvement of the predictions of the model when accounting for NC defects.

# Chapter 6

# Perspectives

The presented two-scale numerical model suffers from the limitations inherent to the QC method. Due to the 2D nature of the available QC software, the method is therefore limited to 2D problems at 0K temperature and when only one GB tilt direction is considered. In other words, this method is applicable to columnar thin films in the case of 0K static equilibrium problems. The two-scale model is however more general even if limited here by the QC hypotheses.

The introduction of nanovoids within the GBs, which constitutes a first step aiming at improving the two-scale model, is not the only defect that should be taken into account. In fact, incorporating kink step defects in GBs would be a very interesting way to improve the model. Auguring futur publications, the first simulation of a GB consisting of one kink has already been undertaken. The illustration of this kink step added in a twin boundary (TB) is given in Figure 6.1. Both TBs, with and without kink step, were subjected to shear loading in the same way as seen previously in Ref. [66]. The curves given in Figure 6.2 were extracted from these simulations in order to evaluate the influence of one kink step on the GB structure. It is found that the interfacial shear strength decreases when the kink is inserted. In short and in the same way as it has been already done in the nanovoids case [66], it should be possible to determine the elasto-plastic laws governing the GBs as a function not only on the kink step concentration but also according to the GB mechanisms involved in the deformation. The resulting new GB laws, corresponding to a decrease of the GB interfacial shear strength, would certainly help leveling the overvaluation problem encountered in the two-scale model presented in this work.

Also, adding calibrated triple junction elements in the continuum should be possible and would allow for a better crack propagation predictions in NCs.

Finite temperature QC, also sometimes referred to "hot-QC method", and able to deal with 3D problems is currently under development by the community. In addition, a recent study [42], which presents a version of the QC code called "Hyper-QC method", is an accelerated finite-temperature QC method enabling longer time scale simulations by coupling the hot-QC with hyperdynamics, already used in MD simulations. The whole two-scale method could thus be recalibrated using the last QC version to integrate the

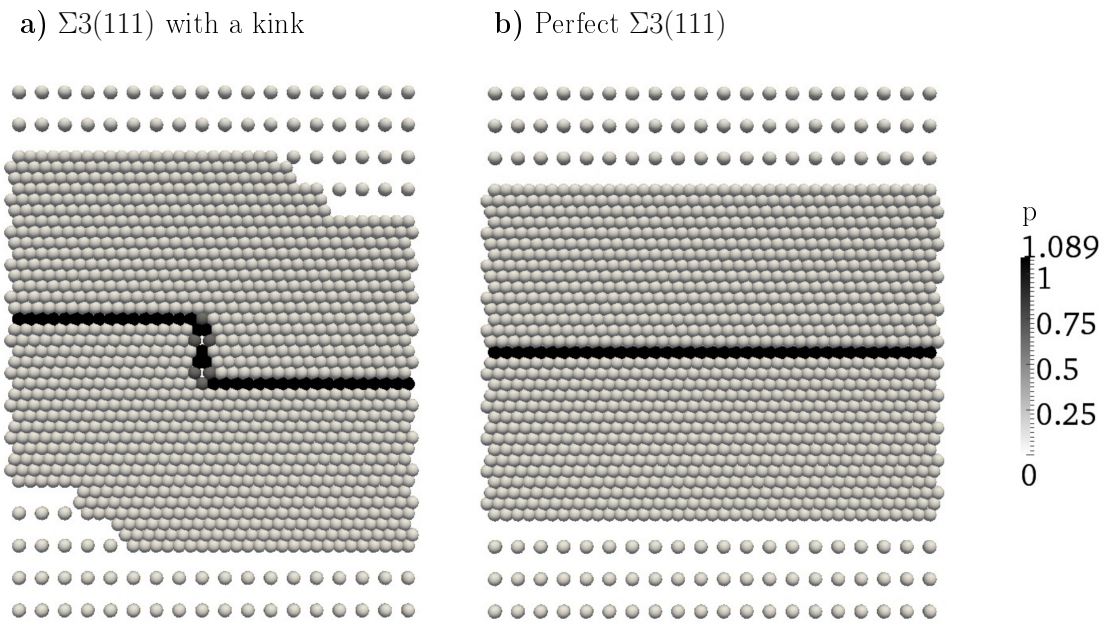


Figure 6.1: QC snaphots of Copper Σ3(111) TB. a) A kink is present. b) Perfect TB. Atoms in bright color have perfect FCC crystal stacking, while dark color atoms correspond to crystal defects.

impact of temperature and 3D effects that are not taken into account in the framework of this work.

The model of plasticity included in the model is a local model, based on the glide of dislocations, for which the grain size effect is taken into account during the calibration process by varying the distance between the indented surface and the GB of the nanoindentation model. The models, presented in Ref. [38, 32, 33, 12, 59], incorporate a dependency on the plastic strain gradients and are capable of capturing size-dependent behavior of metals at the micron scale. Considering these latter non-local frameworks would help to improve the grain plasticity in our two-scale approach.

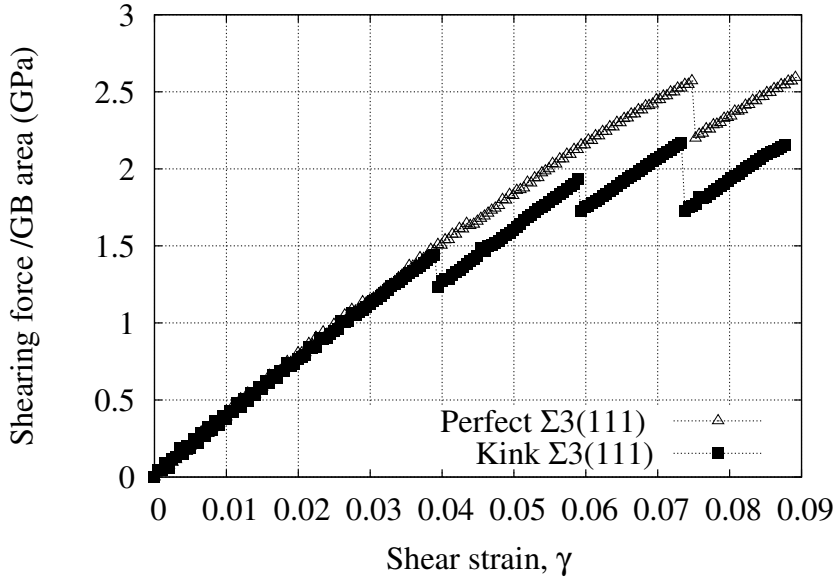


Figure 6.2: Evolution of the shear stress as a function of the applied shear strain for perfect and defective Σ3(111) TBs.

# Bibliography


[1] Alder, B. J., and Wainwright, T. E. Studies in molecular dynamics. i. general method. *The Journal of Chemical Physics 31*, 2 (1959).

[2] Benedetti, I. The boundary element method: Applications in solids and structures. *John Wiley & Sons Ltd., England, vol. 2* (2002).

[3] Benedetti, I., and Aliabadi, M. H. A three-dimensional cohesive-frictional grain-boundary micromechanical model for intergranular degradation and failure in polycrystalline materials. *Computer Methods in Applied Mechanics and Engineering 265* (2013), 36–62.

[4] Brewer, L. N., Othon, M. A., Young, L. M., and Angeliu, T. M. Misorientation mapping for visualization of plastic deformation via electron backscattered diffraction. *Microscopy and Microanalysis 12* (2006), 85–91.

[5] Cahn, J. W., Mishin, Y., and Suzuki, A. Coupling grain boundary motion to shear deformation. *Acta Materialia 54* (2006), 4953–4975.

[6] Cao, A. J., and Wei, Y. G. Atomistic simulations of crack nucleation and intergranular fracture in bulk nanocrystalline nickel. *Physical Review B 76* (2007), 024113.

[7] Changwen, M., Buttry, D. A., Sharma, P., and Kouris, D. A. Atomistic insights into dislocation-based mechanisms of void growth and coalescence. *Journal of Mechanics and Physics of Solids 59* (2011), 1858–1871.

[8] Chen, J., Lu, L., and Lu, K. Hardness and strain rate sensitivity of nanocrystalline cu. *Scripta Materialia 54* (2006), 1913–1918.

[9] Crawford, D. C., and Was, G. S. The role of grain boundary misorientation in intergranular cracking of $Ni_{16}Cr_9fe$ in $360°C$ argon and high-purity water. *Metallurgical and Materials Transactions A 23* (1992), 1195–1206.

[10] Crocker, A. G., Flewitt, P. E. J., and Smith, G. E. Computational modelling of fracture in polycrystalline materials. *International Materials Review 27* (2005), 99–125.

[11] Cuitiño, A. M., and Ortiz, M. Computational modelling of single crystals. *Modelling and Simulation in Materials Science and Engineering 1* (1993), 225–263.

[12] Dahlberg, C. F., and Faleskog, J. Strain gradient plasticity analysis of the influence of grain size and distribution on the yield strength in polycrystals. *European Journal of Mechanics - A/Solids 44*, 0 (2014), 1–16.

[13] Dalla Torre, F., Spätig, P., Schäublin, R., and Victoria, M. Deformation behaviour and microstructure of nanocrystalline electrodeposited and high pressure torsioned nickel. *Acta Materialia 53(8)* (2005), 2337–2349.

[14] De Hosson, J. T. M., Palasantzas, G., Vystavel, T., and Koch, S. Nanosized metal clusters: Challenges and opportunities. *Journal of Materials* (2004), 40–45.

[15] Dobson, M., Elliott, R., Luskin, M., and Tadmor, E. A multiplicative quasicontinuum for phase transforming materials: cascading cauchy born kinematics. *Journal of Computer-Aided Materials Design* (2007).

[16] Donovan, P. E., and Stobbs, W. M. The shear band deformation process in microcrystalline $Pd_{80}Si_{20}$. *Acta Metallurgica 31* (1983), 1–8.

[17] Dupont, V., and Sansoz, F. Quasicontinuum study of incipient plasticity under nanoscale contact in nanocrystalline aluminum. *Acta Materialia 56* (2008), 6013–6026.

[18] Dupuy, L. M., Tadmor, E. B., Miller, R. E., and Phillips, R. Finite temperature quasicontinuum: molecular dynamics without all atoms. *Physical Review Letters 95* (2005), 060202.

[19] El-Sherik, A. M., and Erb, U. Synthesis of bulk nanocrystalline nickel by pulsed electrodeposition. *Journal of Materials Science 30* (1995), 5743–5749.

[20] Fleck, N., and Hutchinson, J. A reformulation of strain gradient plasticity. *Journal of the Mechanics and Physics of Solids 49*, 10 (2001), 2245–2271.

[21] Foiles, S. M., Baskes, M. I., and Daw, M. S. Embedded-atom method functions for the fcc metals $Cu$,$Ag$, $Au$, $Ni$, $Pd$, $Pt$, and their alloys. *Physical Review B 33* (1986), 7983–7991.

[22] Fougere, G. E., Siegel, R. W., Weertman, J. R., and Kim, S. Grain-size dependent hardening and softening of nanocrystalline cu and pd. *Scripta Metallurgica 26* (1992).

[23] Fressengeas, C., Taupin, V., and Capolungo, L. An elasto-plastic theory of dislocation and disclination fields. *International Journal of Solids and Structures 48*, 25-26 (2011), 3499–3509.

[24] Fressengeas, C., Taupin, V., Upadhyay, M., and Capolungo, L. Tangential continuity of elastic/plastic curvature and strain at interfaces. *International Journal of Solids and Structures 49*, 18 (2012), 2660–2667.

[25] Frolov, T., Olmsted, D. L., Asta, M., and Mishin, Y. Structural phase transformations in metallic grain boundaries. *Nature Communications* (2013).

[26] Fu, H. H., Benson, D. J., and Meyers, M. A. Analytical and computational description of effect of grain size on yield stress of metals. *Acta Materialia 49* (2001), 2567–2582.

[27] Fu, H. H., Benson, D. J., and Meyers, M. A. Computational description of nanocrystalline deformation based on crystal plasticity. *Acta Materialia 52* (2004), 4413–4425.

[28] Gianola, D. S., Van Petegem, S., Legros, M., Brandstetter, S., Van Swygenhoven, H., and Hemker, K. J. Stress-assisted discontinuous grain growth and its effect on the deformation behavior of nanocrystalline aluminum thin films. *Acta Materialia 54* (2006), 2253–2263.

[29] Gleiter, H. Nanocrystalline materials. *Progress in Materials Science 33* (1989), 223–315.

[30] Gleiter, H. Nanostructured materials: basic concepts and microstructure. *Acta Materialia 48* (1999), 1–29.

[31] Gurtin, M. E. The burgers vector and the flow of screw and edge dislocations in finite-deformation single-crystal plasticity. *Journal of the Mechanics and Physics of Solids 54*, 9 (2006), 1882–1898.

[32] Gurtin, M. E., and Anand, L. A theory of strain-gradient plasticity for isotropic, plastically irrotational materials. part i: Small deformations. *Journal of the Mechanics and Physics of Solids 53*, 7 (2005), 1624–1649.

[33] Gurtin, M. E., and Reddy, B. D. Gradient single-crystal plasticity within a mises-hill framework based on a new formulation of self- and latent-hardening. *Journal of the Mechanics and Physics of Solids*, 0 (2014), –.

[34] Hall, E. O. The deformation and ageing of mild steel: 3 discussion of results. *Proceedings of the physical Society. Section B 64* (1951), 747.

[35] Hirth, J. P., and Lothe, J. Theory of dislocations. *McGraw-Hill, New York* (1968).

[36] Hughes, G. M., Smith, G. E., Flewitt, P. E. J., and Crocker, A. G. The brittle fracture of polycrystalline zinc. *International Materials Review 463* (2007), 2129–2151.

[37] Hughes, T. J. *The finite element method: linear static and dynamic finite element analysis*. Courier Dover Publications, 2012.

[38] Hutchinson, J. Generalizing j2 flow theory: Fundamental issues in strain gradient plasticity. *Acta Mechanica Sinica 28*, 4 (2012), 1078–1086.

[39] Jérusalem, A., Stainier, L., and Radovitzky, R. A continuum model describing the reverse grain-size dependence of the strength of nanocrystalline metals. *Philosophical Magazine 87* (2007), 2541–2559.

[40] Kelchner, C. L., Plimpton, S. J., and Hamilton, J. C. Dislocation nucleation and defect structure during surface indentation. *Physical Review B 60* (1998), 11085–11088.

[41] Kim, H. S., Estrin, Y., and Bush, M. B. Plastic deformation of fine-grained materials. *Acta Materialia 48* (2000), 493–504.

[42] Kim, W., Luskin, M., Perez, D., Voter, A., and Tadmor, E. Hyper-qc: An accelerated finite-temperature quasicontinuum method using hyperdynamics. *JMPS 63*, 0 (2014), 94 – 112.

[43] Kokawa, H., Watanabe, T., and Karashima, S. Sliding behaviour and dislocation structures in aluminium grain boundaries. *Philosophical Magazine A 44* (1981).

[44] Kraft, R. H., Molinari, J. F., Ramesh, K. T., and Warner, D. H. Computational micromechanics of dynamic compressive loading of a brittle polycrystalline material using a distribution of grain boundary properties. *Journal of Mechanics and Physics of Solids 56* (2008), 2618–2641.

[45] Kuchnicki, S. N., Cuitiño, A. M., and Radovitzky, R. A. Efficient and robust constitutive integrators for single-crystal plasticity. *International Journal of Plasticity 36* (2006), 1.

[46] Kumar, K. S., Van Swygenhoven, H., and Suresh, S. Deformation of electrodeposited nanocrystalline nickel. *Acta Materialia 51* (2003), 387–405.

[47] Kumar, K. S., Van Swygenhoven, H., and Suresh, S. Mechanical behavior of nanocrystalline metals and alloys. *Acta Materialia 51(19)* (2003), 5743–5774.

[48] Kung, H., Sanders, P. G., and Weertman, J. R. Transmission electron microscopy characterization of nanocrystalline copper. *Advanced Materials for the twenty-first Century* (1999), 455–463.

[49] Legros, M., Gianola, D. S., and Hemker, K. J. In situ tem observations of fast grain-boundary motion in stressed nanocrystalline aluminum films. *Acta Materialia 56* (2008), 3380–3393.

[50] Li, J., Wang, Z. L., and Hufnagel, T. C. Characterization of nanometer-scale defects in metallic glasses by quantitative high-resolution transmission electron microscopy. *Physical Review B 65* (2002), 144201–1 144201–6.

[51] Li, Y. S., Tao, N. R., and Lu, K. Microstructural evolution and nanostructure formation in copper during dynamic plastic deformation at cryogenic temperatures. *Acta Materialia 56* (2008), 230–241.

[52] Lin, P., Palumbo, G., Erb, U., and Aust, K. T. Influence of grain boundary character distribution on sensitization and intergranular corrosion of alloy 600. *Scripta Metallurgica and Materialia 33(9)* (1995), 1387–1392.

[53] Lu, K., and Lu, J. Nanostructured surface layer on metallic materials induced by surface mechanical attrition treatment. *Materials Science and Engeneering A* (2004), 38–45.

[54] Lu, L., Shen, Y., Chen, X., Qian, L., and Lu, K. Ultrahigh strength and high electrical conductivity in copper. *Science 15* (2004), 422–6.

[55] Lu, L., Wang, L. B., Ding, B. Z., and Lu, K. High-tensile ductility in nanocrystalline copper. *Journal of Materials Research 15* (2000), 270–3.

[56] Miller, R., and Tadmor, E. B. The quasicontinuum method: overview, applications and current directions. *Journal of Computer-Aided Materials Design 9* (2002), 203–239.

[57] Mühlhaus, H.-B., and Aifantis, E. A variational principle for gradient plasticity. *International Journal of Solids and Structures 28*, 7 (1991), 845–857.

[58] Natter, H., Schmelzer, M., and Hempelmann, R. Nanocrystalline nickel and nickel-copper alloys: Synthesis, characterization, and thermal stability. *Journal of Materials Research 13* (1998), 1186–1197.

[59] Niordson, C. F., and Kysar, J. W. Computational strain gradient crystal plasticity. *Journal of the Mechanics and Physics of Solids 62*, 0 (2014), 31–47. Sixtieth anniversary issue in honor of Professor Rodney Hill.

[60] Ortiz, M., and Pandolfi, A. Finite-deformation irreversible cohesive elements for three-dimensional crack-propagation analysis. *International Journal for Numerical Methods in Engineering 44* (1999), 1267.

[61] Ortiz, M., and Popov, E. P. A statistical theory of polycrystalline plasticity. *Computer Methods in Applied Mechanics and Engineering 90* (1982).

[62] Palumbo, G., and Aust, K. T. Structure-dependence of intergranular corrosion in high purity nickel. *Acta Metallurgica and Materialia 38* (1990), 2343–2352.

[63] Peirce, D., Asaro, R., and Needleman, A. An analysis of nonuniform and localized deformation in ductile single crystals. *Acta Metallurgica 30*, 6 (1982), 1087–1119.

[64] Péron-Lührs, V., Jérusalem, A., Sansoz, F., Stainier, L., and Noels, L. A two-scale model predicting the mechanical behavior of nanocrystalline solids. *Journal of Mechanics and Physics of Solids 61* (2013), 1895–1914.

[65] Péron-Lührs, V., Sansoz, F., Jérusalem, A., and Noels, L. Two-scale computational modeling of intergranular fracture in nanocrystalline metals: Validation and application to low-angle and high-angle textures in nanocrystalline copper. *Computational Materials Science, Under review* (2014).

[66] Péron-Lührs, V., Sansoz, F., and Noels, L. Quasicontinuum study of the shear behavior of defective tilt grain boundaries in cu. *Acta Materialia 64* (2014), 419–428.

[67] Petch, N. J. The cleavage strength of crystals. *Journal of Iron Steel Institute 174* (1953), 25–28.

[68] Rack, H. J., and Cohen, M. Strain hardening of iron-titanium alloys at very large strains. *Materials Science and Engeneering 6* (1970), 320–326.

[69] Randle, V. Twinning-related grain boundary engineering. *Acta Materialia 52* (2004), 4067–4081.

[70] Randle, V. Special boundaries and grain boundary plane engineering. *Scripta Materialia 54*, 6 (2006), 1011–1015. Viewpoint set no. 40: Grain boundary engineering.

[71] Rodney, D., and Phillips, R. Structure and strength of dislocation junctions: an atomic level analysis. *Physical Review Letters 82(8)* (1999), 1704–1707.

[72] Roters, F., Eisenlohr, P., Hantcherli, L., Tjahjanto, D., Bieler, T., and Raabe, D. Overview of constitutive laws, kinematics, homogenization and multiscale methods in crystal plasticity finite-element modeling: Theory, experiments, applications. *Acta Materialia 58*, 4 (2010), 1152–1211.

[73] Rudd, R., and Belak, J. Void nucleation and associated plasticity in dynamic fracture of polycrystalline copper: an atomistic simulation. *Computational Materials Science 24* (2002), 148–153.

[74] Rupert, T. J., Gianola, D. S., Gan, Y., and Hemker, K. J. Experimental observations of stress-driven grain boundary migration. *Science 326* (2009), 1686–1690.

[75] Sailor, D. M., Morawiec, A., Adams, B. I., and Rohrer, G. S. Misorientation dependence of the grain boundary energy in magnesia. *Interface Science 8* (2000), 131–140.

[76] Sansoz, F., and Dupont, V. Grain growth behavior at absolute zero during nanocrystalline metal indentation. *Applied Physics Letters 89* (2006).

[77] Sansoz, F., and Dupont, V. Atomic mechanism of shear localization during indentation of a nanostructured metal. *Materials Science and Engineering C 27* (2007), 1509–1513.

[78] Sansoz, F., and Dupont, V. Nanoindentation and plasticity in nanocrystalline ni nanowires: A case study in size effect mitigation. *Scripta Materialia 63* (2010), 1136–1139.

[79] Sansoz, F., and Molinari, J. F. Incidence of atom shuffling on the shear and decohesion behavior of a symmetric tilt boundary in copper. *Scripta Materialia 50* (2004), 1283–1288.

[80] Sansoz, F., and Molinari, J. F. Mechanical behavior of $\Sigma$ tilt grain boundaries in nanoscale $Cu$ and $Al$: A quasicontinuum study. *Acta Materialia 53* (2005), 1931–1944.

[81] Sansoz, F., and Stevenson, K. D. Relationship between hardness and dislocation processes in a nanocrystalline metal at the atomic scale. *Physical Review B 83* (2011), 224101–1 224101–9.

[82] Schiøtz, J., Di Tolla, F. D., and Jacobsen, K. W. Softening of nanocrystalline metals at very small grain sizes. *Nature 391* (1998).

[83] Schiøtz, J., and Jacobsen, K. W. A maximum in the strength of in nanocrystalline copper. *Science 301* (2003).

[84] Schiøtz, J., Vegge, T., Di Tolla, F. D., and Jacobsen, K. W. Atomic-scale simulations of nanocrystalline metals. *Physical Review B 60* (1999), 11971.

[85] Schwaiger, R., Moser, B., and Dao, M. Some critical experiments on the strain-rate sensitivity of nanocrystalline nickel. *Acta Materialia 51* (2003), 5159–5172.

[86] Shigematsu, N., Prior, D. J., and Wheeler, J. First combined electron backscatter diffraction and transmission electron microscopy study of grain boundary structure of deformed quartzite. *Journal of Microscopy 224* (2006), 306–321.

[87] Shvindlerman, L., and Straumal, B. Regions of existence of special and non-special grain boundaries. *Acta Metallurgica 33*, 9 (1985), 1735 – 1749.

[88] Strachan, A., Cagin, T., and Goddard, W. Critical behavior in spallation failure of metals. *Physical Review B 63* (2001).

[89] Szefer, G., and Jasińska, D. Modeling of strains and stresses of material nanostructures. *Bulletin of the Polish academy of sciences, technical sciences 57* (2009).

[90] Tadmor, E. B., Miller, R., and Phillips, R. Nanoindentation and incipient plasticity. *Journal of Materials Research 14*, 6 (1999), 2233.

[91] Tadmor, E. B., Ortiz, M., and Phillips, R. Quasicontinuum analysis of defects in solids. *Philosophical Magazine A 73* (1996), 1529–1563.

[92] Tadmor, E. B., Smith, G. S., Bernstein, N., and Kaxiras, E. Mixed finite element and atomistic formulation for complex crystals. *Physical Review B 59(1)* (1999), 235–245.

[93] Taupin, V., Capolungo, L., Fressengeas, C., Das, A., and Upadhyay, M. Grain boundary modeling using an elasto-plastic theory of dislocation and disclination fields. *Journal of the Mechanics and Physics of Solids 61*, 2 (2013), 370–384.

[94] Thomas, G. J., Siegel, R. W., and Eastman, J. A. Grain boundaries in nanophase palladium: high resolution electron microscopy and image simulation. *Scripta Metallurgica and Materialia 24* (1990), 201–209.

[95] Valiev, R. Z., Islamgaliev, R. K., and Alexandrov, I. V. Bulk nanostructured materials from severe plastic deformation. *Progress in Materials Science 45* (2000), 103–189.

[96] Van Swygenhoven, H. Microstructure and mechanical behavior of nanocrystalline metals. *Science 296* (2002), 66.

[97] Van Swygenhoven, H., and Derlet, P. M. Grain-boundary sliding in nanocrystalline fcc metals. *Physical Review B 64* (2001).

[98] Van Swygenhoven, H., Spaczér, M., Caro, A., and Farkas, D. Competing plastic deformation mechanisms in nanophase metals. *Physical Review B 60* (1999), 22–25.

[99] Wang, Y. M., , V., H. A., and Ma, E. Defective twin boundaries in nanotwinned metals. *Acta Materialia 54(10)* (2006), 2715–2726.

[100] Warner, D., Sansoz, F., and Molinari, J. Atomistic-based continuum modeling of deformation mechanisms in nanocrystalline copper. *International Journal of Plasticity 22* (2006), 754.

[101] Watanabe, T. An approach to grain boundary design for strong and ductile polycrystals. *Res Mechanica 11* (1984).

[102] Watanabe, T., and Tsurekawa, S. The control of brittleness and development of desirable mechanical properties in polycrystalline systems by grain boundary engeneering. *Acta Materialia 47* (1999), 4171–4185.

[103] Wei, Y., and Anand, L. Grain-boundary separation and sliding: application to nanocrystalline materials. *Journal of Mechanics and Physics of Solids 52* (2004), 2587–2616.

[104] Wei, Y. J., and Su, C. Anand, L. A computational study of the mechanical behavior of nanocrystalline fcc metals. *Acta Materialia 54* (2006), 3177–3190.

[105] Wolf, D., Yamakov, V., Phillpot, S., Mukherjee, A., and Gleiter, H. Deformation of nanocrystalline materials by molecular-dynamics simulation: relationship to experiments. *Acta Materialia 53* (2005), 1–40.

[106] Wrobel, L. C., , and Aliabadi, M. H. The boundary element method: Applications in thermo-fluids and acoustics. *John Wiley & Sons Ltd., England, vol. 1* (2002).

[107] Wu, H. A., Liu, G. R., and Wang, J. S. Atomistic and continuum simulation on extension behaviour of single crystal with nano-holes. *Modelling and Simulation in Materials Science and Engineering 12* (2004), 225–233.

[108] Yamakov, V., Wolf, D., Salazar, M., Phillpot, S., and Gleiter, H. Length-scale effects in the nucleation of extended dislocations in nanocrystalline al by molecular-dynamics simulation. *Acta Materialia 49(14)* (2001), 2713–2722.

[109] Yang, X., Zhou, T., and Chen, C. Effective elastic modulus and atomic stress concentration of single crystal nano-plate with void. *Computational Materials Science 40* (2006), 51–56.

[110] Yip, S. Nanocrystals: the strongest size. *Nature 391* (1998).

[111] Zienkiewicz, O. C., Taylor, R. L., and Zhu, J. Z. *The finite element method: its basis and fundamentals*. Butterworth-Heinemann; sixth edition, 2005.

# Appendix A

# Annex to chapter 2: Paper 1


| | | |
|---|---|---|
| **Author** | : | V. Péron-Lührs, A. Jérusalem, F. Sansoz, L. Stainier, and L. Noels |
| **Title** | : | A two-scale model predicting the mechanical behavior of nanocrystalline solids |
| **Journal** | : | Journal of the Mechanics and Physics of Solids |
| **Year** | : | 2013 |
| **Volume** | : | 61 |
| **Pages** | : | 1895 - 1914 |
| **DOI** | : | 10.1016/j.jmps.2013.04.009 |
| **ISSN** | : | 0022-5096 |
| **Permanent link** | : | http://dx.doi.org/10.1016/j.jmps.2013.04.009 |

# Appendix B

# Annex to chapter 3: Paper 2

| | | |
|---|---|---|
| **Author** | : | V. Péron-Lührs, F. Sansoz, A. Jérusalem and L. Noels |
| **Title** | : | Two-scale Computational Modeling of Intergranular Fracture in Nanocrystalline Copper Metals |
| **Journal** | : | Computational Materials Science, under review |
| **Year** | : | 2014 |

# Appendix C

# Annex to chapter 4: Paper 3


| | | |
|---|---|---|
| **Author** | : | V. Péron-Lührs, F. Sansoz and L. Noels |
| **Title** | : | Quasicontinuum study of the shear behavior of defective tilt grain boundaries in Cu |
| **Journal** | : | Acta Materialia |
| **Year** | : | 2014 |
| **Volume** | : | 64 |
| **Pages** | : | 419 - 428 |
| **DOI** | : | 10.1016/j.actamat.2013.10.056 |
| **ISSN** | : | 1359-6454 |
| **Permanent link** | : | http://dx.doi.org/10.1016/j.actamat.2013.10.056 |